REVISTA MEXICANA DE CIENCIAS GEOLÓGICAS

Revista Mexicana de Ciencias Geológicas, v. 43, num. 1, April 2026, p. 46–64
ISSN-L 2007-2902
https://rmcg.unam.mx

Type: Original research

OPEN ACCESS

Geological and seismological studies in the epicentral region of the major 1887 Sonoran Basin and Range Province earthquake: A project review

Raúl R. Castro[1,a,*], Max Suter[2,b], Gina P. Villalobos-Escobar[3,c], Oscar Romero[4], and Juan Contreras[5,d]

[1] *Departamento de Sismología, División Ciencias de la Tierra, Centro de Investigación Científica y de Educación Superior de Ensenada, Ensenada, Baja California, Mexico.*
[2] *Instituto de Geología, Universidad Nacional Autónoma de México, Estación Regional del Noroeste, Hermosillo, Sonora, Mexico (retired). SuterMax@AlumniBasel.ch.*
[3] *Facultad de Ingeniería Tampico, Universidad Autónoma de Tamaulipas, Tampico, Mexico. gvillalobos@docentes.uat.edu.mx.*
[4] *Facultad de Ciencias de la Tierra, Universidad Autónoma de Nuevo León (UANL), Linares, Nuevo León, Mexico. oscar.romerodlcr@uanl.edu.mx*
[5] *Departamento de Geología, División Ciencias de la Tierra, Centro de Investigación Científica y de Educación Superior de Ensenada, Ensenada, Baja California, Mexico. juanc@cicese.mx.*

** Corresponding autor (R. R. Castro): raul@cicese.mx*
[a] *0000-0003-0463-0117;* [b] *0000-0002-8815-1086;* [c] *0000-0002-7963-8634;* [d] *0000-0002-0409-4337*

How to cite:
Castro, R. R., Suter, M., Villalobos-Escobar, G. P., Romero, O., & Contreras, J. (2026). Geological and seismological studies in the epicentral region of the major 1887 Sonoran Basin and Range Province earthquake: A project review. *Revista Mexicana de Ciencias Geológicas*, *43*(1), 46–64. DOI: https://dx.doi.org/10.22201/igc.20072902e.2026.1.1907

Manuscript received: August 16, 2025
Corrected manuscript received: February 2, 2026
Manuscript accepted: February 2, 2026
Published Online: April 1, 2026

ABSTRACT

A collaborative research project between *Universidad Nacional Autónoma de México* (UNAM) and *Centro de Investigación Científica y de Educación Superior de Ensenada* (CICESE) about the major 1887 earthquake in the Basin and Range Province of northeastern Sonora and the persisting background seismicity in its epicentral region yielded numerous results that are summarized in this paper. Three first-order range-bounding north-south normal faults (from south to north: Otates, Teras, and Pitáycachi) ruptured in this earthquake as evidenced by a multi-segment surface rupture with the maximum vertical displacement of 5.2 m and a length of 102 km, which is the longest extensional dip-slip surface rupture in the worldwide historical record. Empirical scaling relations between surface rupture length and moment magnitude for normal faults estimate a magnitude M_w of 7.5 ± 0.3 for this earthquake. The rupture was arrested in the north as well as in the south at major cross faults, and the rupture displacement profile tapers rapidly toward these faults. The 1887 rupture is characterized at the surface and at focal depth in the mid-to-lower crust by extensional dip slip on 55° to 72°W dipping faults. The rupture kinematics and epicenter of the 1887 earthquake can be inferred from the bilateral branching pattern observed along the trace of the Pitáycachi segment. The focal mechanisms and the inversion of slickenlines exposed on the 1887 surface rupture indicate a normal-fault-type tectonic strain field with an ENE-WSW oriented regional extension. The long-term geological slip rates of the faults that ruptured in 1887 is estimated at 0.02 to 0.08 mm/yr, and the average repeat time of 1887 size ruptures at 15 to 42 kyr.

A regional seismic network, *Red Sísmica del Noreste de Sonora* (RESNES), was installed within this project in the epicentral region of the 1887 earthquake. The network consisted of nine digital autonomous seismological stations and operated from 2002 to 2011. Its recordings indicate ongoing microseismicity not only along the faults that ruptured in 1887, but also along two major Basin and Range Province normal faults located farther south, in the Granados-Huásabas region. In addition to the parametric data of the seismicity distribution, the high quality of the RESNES digital recordings permitted the characterization of the regional seismic attenuation and a spatial analysis of the seismic energy radiated by the recorded earthquakes.

A model of the change in static Coulomb stress throughout this region resulting from the slip on the three individual segments of the 1887 rupture can explain the long-term seismicity pattern

DOI: https://dx.doi.org/10.22201/igc.20072902e.2026.1.1907

in the area. The model suggests that stress increases caused by singularities at the tips of the three rupture segments triggered seismicity in the step-over between the northern and central segments of the surface rupture, as well as in the Granados-Huásabas region, to the south of the documented surface rupture. Furthermore, the model explains the moderate earthquakes that occurred after the 1887 event in the region of the neighboring Fronteras fault. According to the model, these were the result of bending of the hanging-wall blocks of the Pitáycachi and Teras segments.

Keywords: 1887 Sonora earthquake; earthquake surface rupture; local temporary seismic network; microseismicity; regional seismic attenuation; spatial analysis of radiated seismic energy; Basin and Range Province; Sonora; Mexico.

RESUMEN

Un proyecto de investigación en colaboración entre la UNAM y el CICESE del sismo de 1887 del noreste de Sonora y la persistente sismicidad en esta región epicentral proporcionó numerosos resultados que se resumen en este artículo. Tres fallas normales, alineadas escalonadamente en la dirección norte-sur (de sur a norte: Otates, Teras y Pitáycachi), rompieron durante este sismo como es evidenciado por la ruptura superficial de múltiples segmentos con un desplazamiento vertical máximo de 5.2 m y una longitud de 102 km, la mayor longitud de ruptura superficial extensional en el registro histórico mundial. Relaciones empíricas de escalamiento entre la longitud superficial de ruptura y la magnitud para fallas normales proporcionan una estimación de M_w 7.5 ± 0.3. La ruptura fue detenida, tanto en el norte como en el sur, por fallas transversales, y el perfil del desplazamiento de la ruptura se estrechó rápidamente hacia estas. La ruptura de 1887 está caracterizada en la superficie y a profundidad focal, en la corteza media-baja, por un deslizamiento extensional a lo largo de fallas con echados de 55^0 a 72^0 hacia el oeste. La cinemática de la ruptura y el epicentro del sismo de 1887 pueden inferirse del patrón de ramificación bilateral observado a lo largo de la traza del segmento Pitáycachi. Los mecanismos focales y la inversión de estrías expuestas sobre la superficie de la ruptura de 1887 indican un campo de deformación tectónica de falla normal con orientación ENE-OSO de la extensión regional. El porcentaje de deslizamiento a largo-plazo geológico de las fallas que rompieron en 1887 es estimado de 0.02 a 0.08 mm/año, y el tiempo de recurrencia promedio, para un tamaño de ruptura equivalente al de 1887, es de 15 a 42 ka.

Una red sísmica regional, la Red Sísmica del Noreste de Sonora (RESNES), fue instalada en la región epicentral del sismo de 1887. La red consistió en nueve estaciones autónomas digitales que operaron del 2002 al 2011. Los registros de RESNES muestran microsismicidad en curso no solo a lo largo de las fallas que rompieron el 1887, pero también a lo largo de dos fallas normales mayores de la Provincia de Cuencas y Cordilleras localizadas más al sur, en la región de Granados-Huásabas. Además, los parámetros focales de la sismicidad, y la alta calidad de los registros digitales de RESNES permitieron la caracterización de la atenuación sísmica regional y un análisis de la energía sísmica radiada.

Un modelo del cambio en el esfuerzo estático de Coulomb en esta región, como resultado del deslizamiento de los tres segmentos de la ruptura de 1887 puede explicar el patrón de sismicidad a largo-plazo. El modelo sugiere que el incremento del esfuerzo causado por singularidades en los extremos de los tres segmentos que rompieron disparó sismicidad en el escalón entre los segmentos norte y central de la superficie de ruptura, así como en la región de Granados-Huásabas, al sur de la ruptura superficial documentada. Además, el modelo explica los sismos moderados que ocurrieron después del evento de 1887 en la región vecina a la falla Fronteras. De acuerdo con el modelo, estos fueron el resultado de la flexión del bloque de techo de los segmentos Pitáycachi y Teras.

Palabras clave: *Sismo de Sonora de 1887; ruptura sísmica superficial; red sísmica local temporal; microsismicidad; atenuación sísmica regional; análisis espacial de energía sísmica radiada*; *Provincia de Cuencas y Cordilleras; Sonora; México.*

INTRODUCTION

In this article, we review the results of a long-term earthquake-related interinstitutional and interdisciplinary study about the major 1887 Sonoran earthquake and the persisting background seismicity in its epicentral region. The project involved researchers in seismology and numerical tectonic modeling working or studying at *Centro de Investigación Científica y de Educación Superior de Ensenada, Baja California* (CICESE) (Raúl R. Castro, Gina P. Villalobos-Escobar, and Juan Contreras) as well as experts in geology and seismology who were employed at that time at *Instituto de Geología, Universidad Nacional Autónoma de México*, at their *Estación Regional del Noroeste* (ERNO) in Hermosillo, Sonora (Max Suter, César Jacques-Ayala, and Oscar Romero). The project led to numerous publications. In this project review we summarize their highlights, thereby providing a guide for readers who want to look up more details about the subject matter.

Our project built on significant previous studies. Contemporary research about the 1887 earthquake, summarized by Suter (2006), yielded an isoseismal map of the main shock as well as maps and photographs of the surface rupture scarp (see cover image of this issue). On a 10-degree scale, the earthquake had an intensity of X in the epicentral area and was felt over an area of 1 200 000 km^2 (Aguilera, 1888). Significant damage occurred in northwestern Mexico, Arizona, and New Mexico. About a century later, studies undertaken by the University of Arizona and the U.S. Geological Survey mapped the trace of what is known now as the Pitáycachi and Teras segments of the surface rupture (Figure 1), performed a gravity transect across the center of the San Bernardino Valley (hanging wall of the Pitáycachi fault) (Sumner, 1977), and documented in much detail the macroseismic intensity distribution of the mainshock (DuBois and

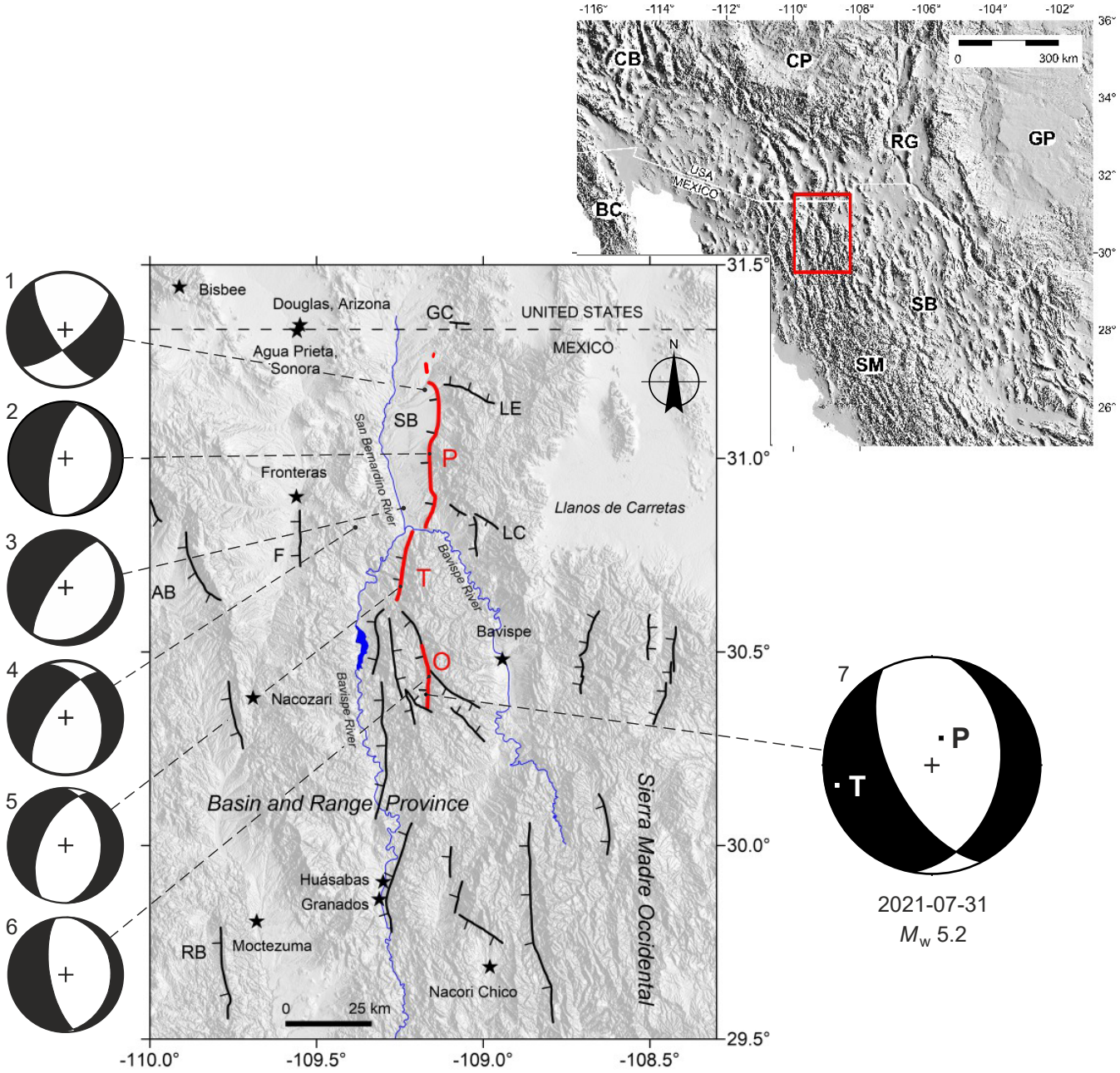

Figure 1. Shaded relief map of northeastern Sonora and northwestern Chihuahua (Mexico) and the adjacent U.S. border region showing in red the 1887 rupture trace (barbs on hanging wall; P, Pitáycachi segment; T, Teras segment; O, Otates segment) and in black the traces of Basin and Range Province as well as pre-Basin and Range faults. SB, San Bernardino Basin; AB, Arizpe Basin; RB, El Rodeo Basin. F, Fronteras fault; GC, Guadalupe Canyon fault; LE, Los Embudos fault; LC, La Cabellera fault. The lower hemisphere equal-area stereoplots represent mean slickenline orientations measured on the rupture surface and earthquake focal mechanisms (P quadrants shaded in grey) (Table 1). The focal mechanism on the right side of the figure represents the 31 July 2021 M_w 5.2 earthquake (Source: Global CMT Catalog), which likely occurred near the southern tip of the Otates fault. Tectonic-physiographic provinces marked on the location map are SM, Sierra Madre Occidental; SB, southern Basin-and-Range; GP, Great Plains; RG, Rio Grande rift; CP, Colorado Plateau; CB, central Basin-and-Range; and BC, Baja California. Modified from Suter (2015).

Smith, 1980), its intensity attenuation (Sbar and DuBois, 1984), and the tectonic geomorphology and Quaternary geology in the epicentral region (Bull and Pearthree, 1988; Pearthree *et al.*, 1990).

The 1887 earthquake has generated a long aftershock sequence, which was recorded in 1978 and 1979 with a portable seismic array by Natali and Sbar (1982) in the region of the Pitáycachi and Teras surface rupture segments. Thirty-three earthquakes were detected during thirty days of usable recording. The most accurate locations (horizontal error ≤5 km) defined a west-dipping, normal, range-bounding fault, and all events occurred within 15 km of the surface. The recorded seismicity terminated abruptly 13 km to the north of the Pitáycachi segment but extended in the south for at least 32 km beyond the southern limit of the Teras segment. This pioneer study raised new questions about the active tectonics of northeastern Sonora, especially whether the 1887 rupture actually extended farther south and whether there are more faults with Quaternary activity in that region. To answer

these questions and to monitor the current seismicity in eastern Sonora, we installed in 2002 a regional seismic network consisting of nine stations in the epicentral region of the 1887 earthquake, named *Red Sísmica del Noreste de Sonora* (RESNES), which operated until 2011. Besides providing data about the seismicity distribution, the high quality of the RESNES digital recordings also offered a valuable opportunity to characterize the seismic attenuation in northeastern Sonora and to study the distribution of the radiated seismic energy.

Prior to the RESNES installation, we compiled the historical seismology of northeastern Sonora and northwestern Chihuahua in form of an earthquake catalog. We then mapped the geology in the epicentral region of the major 1887 Sonora earthquake and made detailed structural and morphological field measurements of its surface rupture. Our field observations permitted an estimate of the geologic slip rates and recurrence intervals of the faults involved in the 1887 rupture and served as a base for the lay-out of the RESNES network and for a numerical model of the changes in the tectonic stress field caused by the 1887 rupture.

TECTONIC SETTING

Northeastern Sonora, which is part of the Basin and Range tectonic–physiographic province, is characterized by numerous, generally north–south-striking map-scale subvertical faults (Figure 1). This extension initiated *circa* 25 Ma (late Oligocene), as indicated by the age of basalt flows intercalated with the lowermost fill of the associated basins, such as the Arizpe and El Rodeo Basins (Figure 1), which are mostly half-grabens. Subsidence occurred mostly between 25 Ma and 18 Ma, at a rate of ~0.5 mm/yr (González-León *et al*., 2010). A cross-sectional reconnaissance in the central part of Figure 1 indicates 10% east-west extension caused by subvertical north-south striking normal faults with throws of 1-2 km (Suter, 2008a).

Additionally, northeastern Sonora is affected by regional-scale NW-SE striking high-angle pre–Basin-and-Range normal faults. In the region of the Otates fault (Figure 1), these faults have throws of 300–600 m, cause a regional extension of 4%, and are more narrowly spaced than the major Basin-and-Range faults (Suter, 2008a). This 30–23 Ma NE- SW crustal extension was prevalent over a vast area of what is now the southern Basin and Range province and the southern Rio Grande rift (inset to Figure 1), reaching as far south as central Mexico (Suter and Morelos-Rodríguez, 2025, and references therein).

Three first-order range-bounding north-south normal faults (from south to north: Otates, Teras, and Pitáycachi) ruptured in the 1887 Sonora earthquake as evidenced by a multi-segment surface rupture (marked in red in Figure 1) with maximum vertical displacement of 5.2 m and a length of 102 km (Table 1), which is the longest extensional dip-slip surface rupture in the worldwide historical record (Schwartz, 2018). At the same time, these are the only Basin and Range Province faults in Mexico with known historical coseismic surface rupture. Empirical scaling relations between surface rupture length and moment magnitude for normal faults (Wells and Coppersmith, 1994) estimate a magnitude M_w of 7.5 ± 0.3 for this earthquake. Several more earthquakes of lesser magnitudes originated in the epicentral region of the 1887 Sonora earthquake in the early twentieth century (Suter, 2001). More recently, an M_w 5.2 event originated on 31 July 2021 near the southern tip of the Otates segment of the 1887 surface rupture (Ben-Horin and Pearthree, 2021) (Figure 1, Table 2).

The focal mechanisms of earthquakes in the epicentral region of the 1887 main shock all indicate normal faulting at mid-to-lower crustal depth on approximately north–south-striking planes. The focal mechanisms and the inversion of slickenlines exposed on the 1887 surface rupture (Figure 1, Table 2) indicate a normal-fault-type tectonic strain field with an ENE-WSW oriented regional extension. The same fault pattern and tectonic strain field characterizes most of northern Mexico (Suter and Morelos-Rodríguez, 2025) and the adjacent part of the United States (U.S. Geological Survey, 2025; Hatem *et al.*, 2022, and references therein) and extends in the south to the Trans-Mexican volcanic belt, where it is overprinted by a regional-scale system of east–west striking, seismically active normal faults that are oriented parallel to the axis of this volcanic arc (Suter, 2020; Suter and Morelos-Rodríguez, 2024, and references therein).

Farther north, in the United States part of the Basin and Range Province, an east-northeast–west-southwest-oriented Quaternary bulk extension (Broerman *et al*., 2021) with a rate of ~0.12 mm/yr (Berglund *et al*., 2012) has been modeled based on Global Positioning System velocities. The Quaternary bulk extension and the extension rate in the Basin and Range Province of northern Mexico remain to be documented but are likely to be of a similar magnitude. Significant Basin and Range Province earthquakes to the north of the 1887 Sonora rupture are the 2014 M_w 5.3 Duncan, Arizona earthquake (Young and Pearthree, 2014) and the 1938 M 5.5 Glenwood, New Mexico earthquake (Gutenberg and Richter, 1949; Taggart and Baldwin, 1982) on the western, fault-bounded margin of the Mogollon mountains.

SURFACE RUPTURE OF THE 1887 MAIN SHOCK

Our detailed fieldwork in the epicentral region of the 1887 main shock focused on mapping the trace of its surface rupture scarp.

Table 1. Structural parameters of the 1887 Sonora earthquake surface rupture (from Suter, 2015).

Segment	Length (km)	Northern endpoint		Southern endpoint		Strike (°)	Average Dip (°W)	Maximum surface offset (m)	Average surface offset (m)	Maximum slip (m)	Average slip (m)	Recurrence interval (kyr)	Long-term slip rate (mm/yr)
		Long (°W)	Lat (°N)	Long (°W)	Lat (°N)								
Víbora-North	0.8	109.149	31.270	109.151	31.263	15.6	—	0.46	0.39[a]	—	—	—	—
Víbora-South	2.1	109.173	31.242	109.168	31.223	-13.3	—	0.49	0.43[a]	—	—	—	—
Pitáycachi	41.0	109.159	31.194	109.180	30.825	2.0	70	4.87	2.60[b]	5.16	2.77	100–200[c]	0.06
Teras	20.0	109.212	30.810	109.259	30.635	12.0	62[d]	1.84	1.12[b]	2.08	1.27	15–26	0.08
Otates	18.2	109.184	30.516	109.168	30.352	-5.8	68	2.50	1.75[b]	2.70	1.89	30–42	0.06
Entire Rupture	101.8	109.149	31.270	109.168	30.352	0.1	69	4.87	1.97	5.16	2.11	—	—

Note: Recurrence interval refers to the average repeat time of 1887-sized ruptures. [a] Arithmetic mean. [b] Based on integration of regression function. [c] During the Quaternary based on Bull and Pearthree (1988). [d] Since no slickensides were observed on the free face of the Teras rupture segment, the average dip measured on the Teras fault plane is given as a proxy.

Table 2. Slip Parameters and P- and T-axes from slickenlines on the 1887 rupture and focal mechanisms (from Suter, 2015, modified).

Reference	Rupture segment	Long (°W)	Lat (°N)	Strike (°)	Dip (°W)	Rake (°)	Type of motion	*P* axis		*T* axis		Type of measurement	Source
								Trend (°)	Plunge (°)	Trend (°)	Plunge (°)		
1	Pitáycachi[a]	109.177	31.178	148	70	−158	N-RL	10	30	100	0	CFM	Natali and Sbar (1982)
2	Pitáycachi	109.162[b]	31.013[b]	193	69	−88	N-LL	108	66	281	24	S	Suter (2015)
3	Pitáycachi[c]	109.240	30.872	215	72	−90	N	125	63	305	27	CFM	Natali and Sbar (1982)
4	Teras[d]	109.389	30.823	216	65	−58	N-LL	170	57	283	14	FM	Wallace and Pearthree (1989)
5	Teras[e]	109.250[b]	30.670[b]	204	55	−82	N-LL	160	75	283	8	S	Suter (2008a)
6	Otates	109.164[b]	30.437[b]	170	68	−94	N	71	67	264	23	S	Suter (2008b)
7	Otates[f]	109.17	30.39	153	59	−111	N-RL	18	69	258	11	FM	Global CMT Catalog

Note: The parameters are based on the convention by Aki and Richards (2002). The references are listed from north to south and marked on Figure 1, where the parameters are also graphed. [a] Near northern end of Pitáycachi surface rupture segment. [b] Midpoint on the rupture trace between outermost slickenline measurement sites. [c] Near southern end of Pitáycachi surface rupture segment. [d] Focal mechanism for the 25 May 1989 M 4.2 earthquake, which possibly had its source on the Teras fault. [e] Slickenlines measured on the Teras fault plane are given here as a proxy, because no slickenlines were observed on the 1887 free face of the Teras rupture segment. [f] Focal mechanism for the 31 July 2021 M_w 5.2 earthquake, which likely had its source on the Otates fault. N: normal; N-RL: normal–right-lateral; N-LL: normal–left-lateral. CFM: composite focal mechanism; S: slickenlines; FM: focal mechanism; CMT: Centroid Moment Tensor.

Additionally, we measured at numerous sites the scarp width, scarp height, the preserved height, and orientation of its free face (*i.e.*, the part of the scarp surface being steeper than the angle of repose), and the coseismic slickenlines on the scarp surface. The surface offset (vertical separation of the ground surface) was calculated from the scarp height and the slope angle above and below the scarp. Geological maps with the surface rupture trace and the measurement sites as well as the measurements themselves were published individually for each rupture segment (Suter, 2008a, 2008b, 2015) and are also available online (see Data and Resources).

Otates rupture segment

Along the Basin and Range Otates fault, which forms a pronounced linear fault escarpment (Suter, 2008a), the 1887 rupture scarp is well exposed (Figure 2) but was not previously studied, due in part to its location in a remote mountain region within a large horseshoe-shaped bend of the Bavispe river (Figure 1), in an area without permanent population and inaccessible by vehicle. The surface rupture coincides with the mapped trace of the Otates fault, dips 68°W, and has an end-point-to-end-point length of 18.2 km (Table 1). The lateral rupture terminations are controlled by NW-SE striking pre–Basin-and-Range cross faults (Figure 1). Coseismic slickenlines (Table 2) and the style of rupture indicate extensional dip slip without significant lateral displacement. Based on measurements of the surface deformation at 25 sites (Suter, 2008a), the maximum slip along the Otates fault in the 1887 earthquake was 270 cm, and the average slip was 189 cm. The along-rupture surface offsets indicate an asymmetric distribution with the maximum offset near the northern end of the rupture segment (Figure 3), which can be explained by the mechanical interaction of the Teras and Otates surface-rupture segments through their stress fields. A long-term geological slip rate of 0.06 mm/yr can be inferred from the structural geometry of the Otates fault (average

Figure 2. Eastward view from near Los Otates ranch showing silicic volcanic rocks of the Sierra El Tigre, the Otates fault, and remnants of the 1887 rupture scarp (indicated by arrows at sites 18 to 21; the site numbers refer to table 1 and fig. 4 in Suter, 2008a). Photograph taken in 1997 by Max Suter. From Suter (2008a).

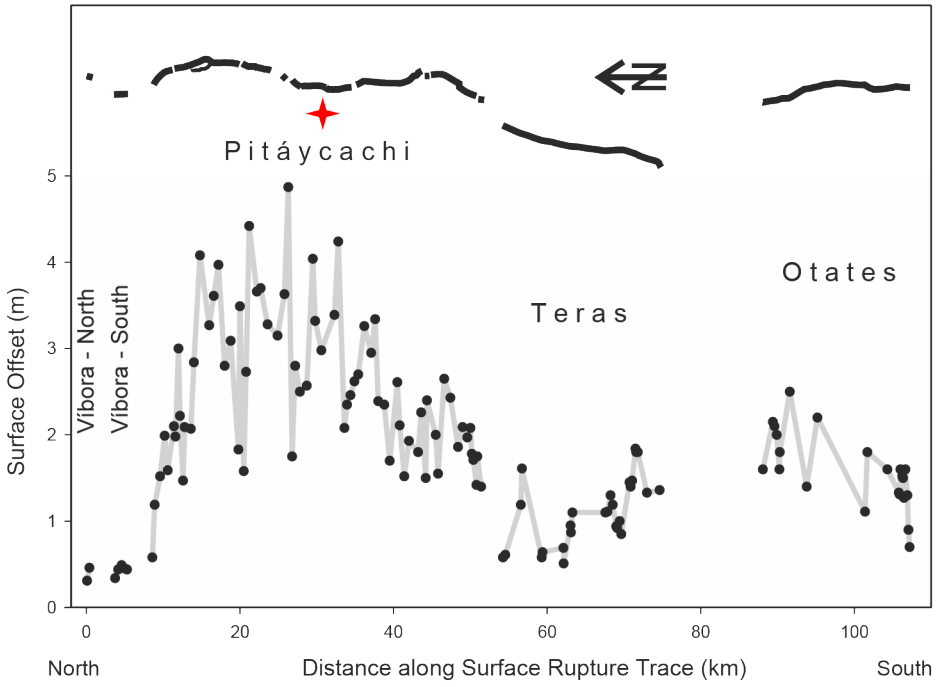

Figure 3. Fault trace map (upper part of figure, with North to the left) and surface offset scatter diagram of the entire 1887 earthquake rupture. The star marks the estimated location of the 1887 main shock epicenter. From Suter (2015).

dip and throw of the limit between the Oligocene felsic and mafic volcanic rock units, which are mappable across the fault) and the assumption that the regional extension initiated ~25 Ma ago. The average recurrence interval of 1887-sized earthquakes on the Otates fault is 30–42 kyr based on this long-term geologic dip-slip rate and its amount of slip in the 1887 earthquake (Table 1).

Teras rupture segment

Like the Otates fault, the Teras fault forms a pronounced linear fault escarpment, and the 1887 rupture scarp along the fault is well exposed (Suter, 2008b). Slip vector measurements on the Teras fault plane (Table 2), a proxy for the 1887 slip vector on the Teras rupture segment, indicate dip slip with a minor left-lateral strike-slip component. Similarly, the focal mechanism obtained by Wallace and Pearthree (1989) for the 25 May 1989 M 4.2 earthquake (Table 2), which probably had its source on the northern part of the Teras fault (Figure 1), indicates dip slip with a minor left-lateral strike-slip component on the 65°W dipping nodal plane.

The 1887 surface rupture coincides with the mapped trace of the Teras fault (Figure 1), which dips 62°W, and has an end-point-to-end-point length of 20.0 km. Based on measurements of the surface deformation at 27 sites, the maximum slip along the Teras fault in the 1887 earthquake was 184 cm, and the average slip was 112 cm (Table 1). The along-rupture surface offsets indicate an asymmetric distribution with the maximum offset near the southern end of the rupture segment (Figure 3). The average recurrence interval of 1887-sized earthquakes on the Teras fault is 15–26 kyr based on the long-term geologic dip-slip rate of the fault (0.08 mm/yr) and its amount of slip in the 1887 earthquake (Table 1).

The segment boundary between the Teras and Otates faults is characterized by a basement ridge and a fault relay zone where the displacement of the Teras fault is transferred onto the Otates fault and two more normal faults to the west of it (Figure 1; DuRoss *et al.*, 2016, their fig. 9). The basement ridge formed a structural barrier, which at its surface was not breached by the 1887 rupture. Digital terrain models and geological maps of that region can be found in the papers about the Otates and Teras rupture segments (Suter, 2008a, 2008b).

A 2.5-km-wide, unbreached right step-over separates the Pitáycachi and Teras segments of the 1887 earthquake surface rupture across the Bavispe river (Figure 1). This step-over is also defined by a minimum in the 1887 slip distribution (Figure 3), which suggests that the Pitáycachi and Teras are independent rupture segments that do not merge at depth. In their approach to the step-over, the traces of the Pitáycachi and Teras rupture segments are characterized on a smaller length scale by right-stepping en-échelon patterns (Suter, 2008b, fig. 2; Suter, 2015, fig. 3) indicating a distributed left-lateral component of motion within this transfer zone.

Pitáycachi rupture segment

The Pitáycachi fault strikes approximately north-south, and its average dip at the surface is 72°W (Suter, 2015). An identical dip can be inferred from the composite focal mechanisms of microearthquakes located west of the Pitáycachi fault trace (Figure 1) (Natali and Sbar, 1982), which suggests that the fault has a constant steep dip down to mid-crustal levels. The footwall of the Pitáycachi fault (Figures 4 and 5) is more back eroded and embayed than the footwalls of the Otates (Figure 2) and Teras faults. For that reason, the trace of the Pitáycachi fault is morphologically less conspicuous. Pliocene to early Pleistocene (2 Ma–750 ka) braided-stream deposits are vertically displaced by the Pitáycachi fault up to 60 m (Suter, 2015), indicating a slip rate in the range between 0.03 and 0.08 mm/yr. These values are comparable to the geological slip rates of the Teras and Otates faults (0.06 and 0.08 mm/yr, respectively, Table 1).

The 1887 surface rupture scarp along the Pitáycachi fault is still well exposed (Figures 4 and 5). It has an endpoint-to-endpoint length of ≥41.0 km, dips ~70°W, and is characterized by normal left-lateral extension. Measurements of the surface deformation were made at 96 sites (Suter, 2015), including seven sites on the minor Víbora segments,

Figure 4. Surface rupture (low white ribbon) along the central part of the Pitáycachi rupture segment, seen from the WNW. The scarp height is approximately four meters. Background: volcanic rocks of the Sierra Madre Occidental; middle ground (foothills of the Sierra Madre): Cretaceous Mural limestone; foreground: alluvial fan deposits of the San Bernardino valley. Photograph taken in 1999 by Max Suter. From Suter (2015).

located farther north (Figures 1 and 3). The maximum surface offset is 487 cm and the mean offset 260 cm (Table 1).

Unlike the 1887 surface rupture along the Otates and Teras faults, which is not significantly segmented along strike, the Pitáycachi segment has subsidiary faults, branches that splay off the main rupture on either side at angles between 20 and 40°, and a complex pattern of second-order segmentation (Suter, 2015). However, this segmentation is not expressed in the 1887 along-rupture surface offset profile (Figure 3), which indicates that the secondary segments are linked at depth into a single coherent fault surface. The width of the rupture zone is typically narrow (1–5 m) but can be wider (up to 2 km) near the bifurcations and links between second-order segments.

RUPTURE KINEMATICS

It is remarkable that the rupture kinematics and the epicenter of this pre-instrumental earthquake can be inferred from surface structural observations such as rupture branching and the slip distribution. The Pitáycachi surface rupture shows a well-developed branching pattern consisting of at least six north facing bifurcations in the northern part of the segment and two south facing bifurcations in its southern part (Suter, 2015). In analog experiments of branching ruptures, the bifurcations are consistently in the direction of rupture propagation (Bahat, 1982; Sharon et al., 1995; Sharon and Fineberg, 1999; Bouchbinder et al., 2010). The orientation of the bifurcations can therefore be taken as an indicator of the direction of rupture propagation, and the change in directionality may indicate where the rupture initiated. This fracture mechanics interpretation of the branching pattern suggests that the rupture of the Pitáycachi segment originated in its central part (Figure 3), where the direction of the rupture bifurcations changes.

Most remarkable is the sprouting of several branches in the northern part of the Pitáycachi rupture segment (Suter, 2015, his figs. 3 and 8). The individual branches formed on either side of the main rupture, and all the bifurcations open to the north. Based on the

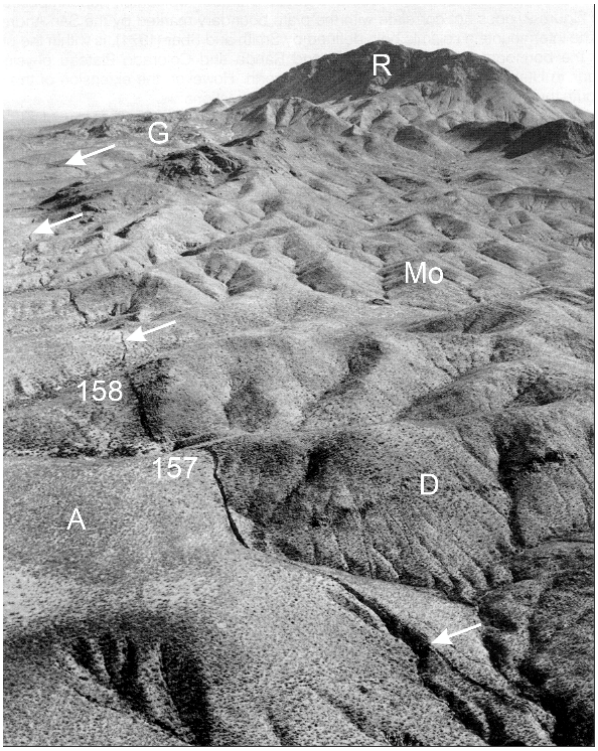

Figure 5. Looking north along the 1887 rupture scarp (white arrows) in the central part of the Pitáycachi segment (modified from DuBois & Smith, 1980; oblique aerial photograph taken by Peter Kresan). The rupture separates bedrock in the footwall from piedmont alluvium in the hanging wall. In the foreground, the surface offset is 261 cm at site 158 and 174 cm at site 157 (The site numbers refer to table 2 and fig. 3 in Suter, 2015). Note the south-facing rupture bifurcation in the right foreground marked by an arrow. A: piedmont alluvium; R: rhyolite (Cerro Pitáycachi); Mo: La Morita Formation (east-dipping siliciclastic rocks); G: granite; D: dike within La Morita Formation. The distance between the foreground and Cerro Pitáycachi is ~20 km. From Suter (2015).

directionality of its branching pattern, the rupture is inferred to have propagated here from south to north. The rupture front separated the ground surface vertically by 4 m before becoming unstable and distributing into several branches. Most of the branches die out after a relatively short distance. The through-going major rupture has a low surface offset where it passes along the branches but gains again more offset farther north, beyond the branch tips. Similar branching patterns have been observed in millimeter-scale analog experiments in brittle materials (Sharon *et al.*, 1995). A dynamic instability occurs as the speed of a crack increases beyond a critical value (typically 0.4 times the speed of Raleigh waves), at which a crack will change its topology as it sprouts short-lived side branches. As in the observed 1887 branching pattern, the experimental branches, in general, do not appear as a single side branch but in bunches that progressively become more complex as the mean crack velocity increases (Sharon *et al.,* 1995). Because a rupture is driven by the energy flux to its tip, the formation of a new branch decreases the amount of energy flowing into the main rupture, thereby reducing its velocity (Broek, 1986). Conversely, the death of a branch causes the main rupture to accelerate, as more energy is available to drive it. This results in fluctuations in the velocity of the rupture front, with a timescale characteristic of a branch lifetime (Sharon and Fineberg, 1999). Our observations in conjunction with these millimeter-scale experimental results suggest that the properties of branching instabilities are length scale independent and that the measured surface offsets (and implicitly slip) within the documented 1887 branching pattern correlate with the fluctuations in rupture velocity.

Most likely the rupture first propagated bilaterally along the Pitáycachi fault. The southern rupture front likely jumped across a step over to the Teras fault and from there across a major relay zone to the Otates fault (Suter, 2015). The postulated rupture path is in agreement with the intensity distribution of this earthquake (Aguilera, 1888; Sbar and DuBois, 1984), which suggests a strong rupture directivity effect towards the south. Branching probably resulted from the lateral propagation of the rupture after breaching the seismogenic part of the crust, given that the much shorter ruptures of the Otates and Teras segments did not develop branches.

HISTORICAL EARTHQUAKES

One of the main tasks at the beginning of the project was the compilation of a parametric database of historical earthquakes in northeastern Sonora and northwestern Chihuahua based on an exhaustive search for earthquake-related information in newspapers, archives, and publications at Hemeroteca Nacional de México, Hemeroteca de la Universidad de Sonora, Arizona Historical Society, University of Arizona (Main Library), Instituto Chihuahuense de la Cultura (Archivo Histórico), and Archivo General del Estado de Sonora (Suter, 2001). As a correction to that article, it should be noted that the 28 October 1965 Nicolás Bravo, Chihuahua ($m_b = 5.0$) earthquake, mentioned even in its abstract, was most likely a mine blast. Its epicenter (28.183° N / 108.400° W), as indicated by Figueroa (1970) (source: United States Coast and Geodetic Survey), is located exactly at Mina de Ocampo, which shows on satellite imagery as a large open pit mine.

The database was used for the graphical visualization of the seismicity distribution on contour maps and shaded-relief maps. Isoseismal maps were constructed for several earthquakes, such as the 1907 Colonia Morelos shock (Figure 6). The magnitude of

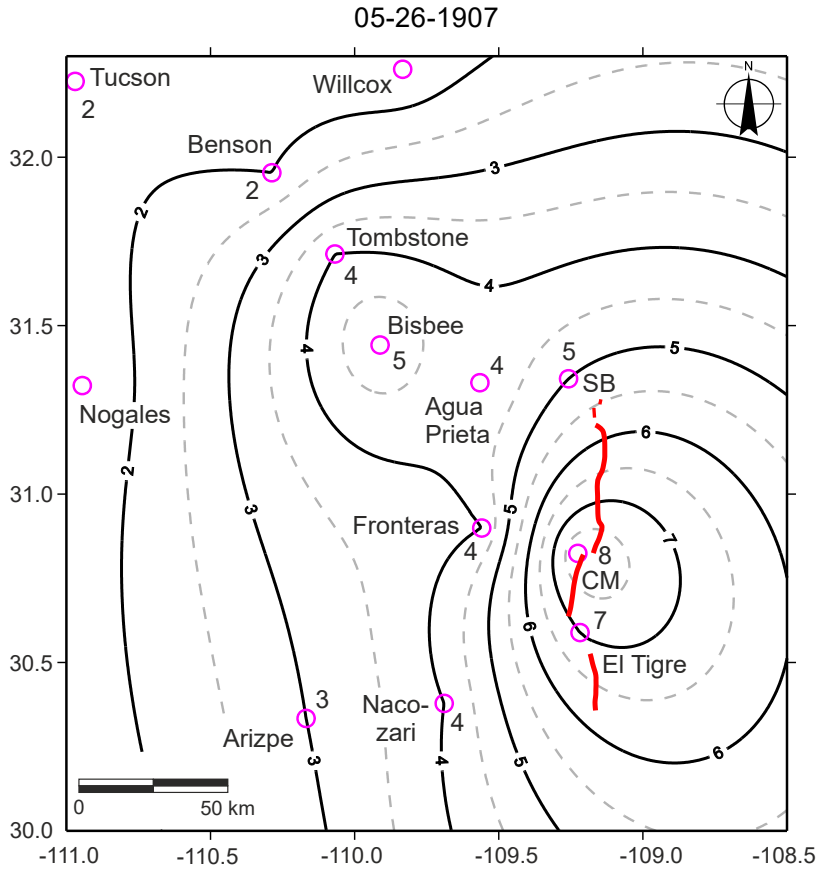

Figure 6. Isoseismal map for the 26 May 1907 earthquake. SB, San Bernardino Ranch; CM Colonia Morelos. The trace of the 1887 surface rupture is marked in red. Modified from Suter (2001).

these events was estimated based on established regressions between instrumentally recorded magnitudes and the maximum intensity and intensity distributions of shallow normal fault earthquakes in the southern Basin and Range Province and the Trans-Mexican volcanic belt (Suter *et al*., 1996).

No information was found about historical earthquakes in northeastern Sonora prior to the 1887 event. Moderate earthquakes occurred after the 1887 main shock in the region of the step-over between the northern and central segments of the 1887 surface rupture (26 May 1907 Colonia Morelos, Sonora, I_{max} VIII, M_I 5.2±0.4, Figure 6; 25 May 1989, M 4.2, Figure 1 and Table 1); in the region of the Fronteras fault (Figure 1) (7 April 1908, M_I 4.8); and in the Granados-Huásabas region (Figure 1), to the south of the documented 1887 surface rupture 17 May 1913 (I_{max} VIII, M_I 5.0±0.4) and 18 December 1923 (I_{max} IX, M_I 5.7±0.4).

Based on several letters of the Huásabas Municipal Council to the Sonora State Government in Hermosillo, a strong shock on 17 May 1913, at 2 a.m. local time destroyed a third of the buildings in Huásabas (Figure 1) and caused major damage to the townhall, schoolhouse, and prison. The shocks, about 40 in all, caused the population to leave their homes and camp in the open.

Based on documents preserved at Archivo General del Estado de Sonora (facsimiles are online; see Data and Resources), a relatively short shock on 18 December 1923, 5 a.m. local time, destroyed most adobe constructions in Huásabas (Figure 1) and Granados. A second major shock on 19 December 1923, 6 a.m. local time razed the two villages and was followed by 27 aftershocks on the same day and by more aftershocks that lasted at least until April 1924. The 1913 and 1923 earthquakes had a small felt area but were locally devastating, which can be explained by amplification of ground shaking in the alluvium of the Bavispe river underlying Granados and Huásabas and a shallow focal depth. The earthquakes may have originated on the Basin and Range fault that forms a pronounced scarp just east of these two towns (Figure 1).

The 1913 M_I 5.0 and 1923 M_I 5.7 earthquakes in the Granados-Huásabas region, the recent microseismicity recorded by the RESNES array (outlined below), and the 2021 M_w 5.2 earthquake near the southern tip of the Otates fault (Figure 1) indicate that the area of aftershock activity of the 1887 earthquake has increased southward with time. This may be related to the southward direction of the 1887 rupture propagation proposed above and the related rupture directivity effect.

COULOMB STRESS MODELLING

The change in Coulomb failure stress caused by the rupture of individual segments of a fault zone may advance or delay the rupture of adjacent segments (King *et al.,* 1994). This suggests that the various segments of the fault zone on the western edge of the Sierra Madre Occidental plateau (Figure 1) may have failed in the past in segment combinations that are different from the one that ruptured in 1887 (Pitáycachi–Teras–Otates), which probably results in major fluctuations of the recurrence intervals for the individual fault segments.

A model of the change in static Coulomb stress throughout this region (Figure 7) resulting from the slip on the three individual segments of the 1887 rupture (Suter and Contreras, 2002) can explain the long-term seismicity pattern in the area. The slip planes of the faults are represented by three subparallel, west-dipping elastic screw-dislocations oriented N-S. The model suggests that stress increases caused by singularities at the tips of the three rupture segments (Figure 7) triggered seismicity in the step-over between the northern and central segments of the surface rupture, as well as in the Granados-Huásabas region, to the south of the documented surface rupture. This long-term seismicity is driven by post-seismic mantle relaxation and stress transfer associated with the elastic deformation induced by the rupture (Pollitz and Cattania, 2017).

Note that not all aftershocks occur within zones of Coulomb stress buildup. The discrepancy can be explained by small-scale fault heterogeneities not included in the model, fluid-pressure changes, and viscoelastic relaxation, among other factors (Pollitz and Cattania, 2017). Furthermore, the model explains the moderate earthquakes that occurred after the 1887 event in the region of the neighboring Fronteras fault (Figure 1), likely resulting from hanging-wall adjustment after the 1887 mainshock by normal faults in the hanging-wall blocks of the Pitáycachi and Teras segments (*e.g.*, Liang *et al.* 2022).

THE SEISMIC NETWORK OF NORTHEASTERN SONORA (RESNES)

The RESNES array (Castro *et al.*, 2002; Romero *et al.*, 2004) consisted of nine digital recorders with Episensors recording the 3 components of ground acceleration with a sample rate of 200 Hz and, with an additional channel, the vertical ground motion velocity-component from an external short-period seismometer. The RESNES recorders also had a built-in GPS timing system for time control.

The stations of the RESNES seismic network were initially installed mainly around the Pitáycachi fault (Figure 8), the northern segment of the fault system that ruptured during the 1887 earthquake. A few months after the initial installation, we realized that most of the recorded local seismicity concentrated near the southern end of the Pitáycachi fault and farther south, near the Teras and Otates faults. For this reason, we relocated the stations and extended the array to the south. To have a better control of the regional seismicity, we also used records of the RESBAN array (*Red Sismológica de Banda Ancha del Golfo de California*), operated by CICESE and NARS (Network of Autonomously Recording Seismographs) (Trampert *et al*., 2003; Clayton *et al.*, 2004). During the operating period of the RESNES array, there were EarthScope Transportable USArray stations operating north of the border (Figure 8), whose records we also used for hypocenter location purposes (Castro *et al*., 2010). The seismicity within Arizona during the deployment of the USArray seismic stations was analyzed by Lockridge et al. (2012). For the installation of the RESNES stations we selected mostly rock or hard-soil sites to avoid the contamination by ambient noise. Figure 9 shows a sample of velocity seismograms recorded at stations OAX, ELO, and OJO from an earthquake located on the Pitáycachi fault.

THE AFTERSHOCK SEQUENCE OF THE 1887 (Mw7.5) EARTHQUAKE

The long-lasting aftershock sequence generated by the 1887 earthquake is likely the result of low slip rates of the faults that ruptured, the large magnitude of the mainshock and the long recurrence times of these faults (Castro *et al.*, 2010). Mechanical models predict that the recurrence time of large earthquakes is proportional to the seismicity production (Dieterich, 1994). The recurrence time of the Pitáycachi fault, for instance, is 100–200 k.y. (Bull and Pearthree, 1988), and this long recurrence time consequently reduces the seismic hazard related to great earthquakes but because of the long aftershock duration, the hazard related to moderate magnitude events will persist for longer time in the Sonora Basin and Range and beyond.

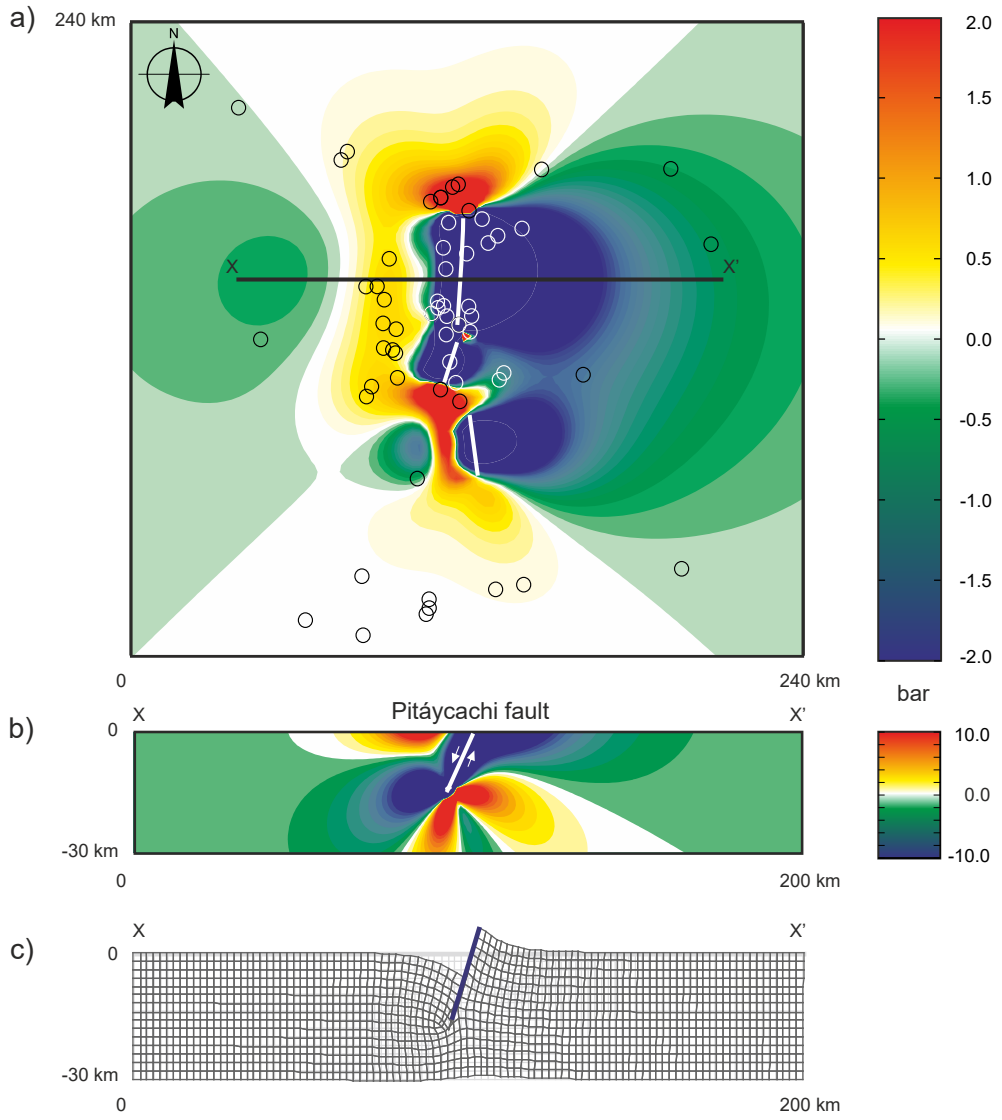

Figure 7. (a) Model of the changes in Coulomb failure stress resulting from the 1887 rupture (white line), at a depth of 7 km on north-south striking faults with a dip of 75°W. Lobes of stress increase can be observed at the tips of the 1887 rupture segments. Stress build-up is also notable in the region of the Fronteras fault (Figure 1). The circles represent the epicenters documented in Suter & Contreras (2002; their fig. 2). The same source also provides information on the model parameters. (b) Cross section of the changes in Coulomb failure stress near the Pitáycachi segment of the 1887 rupture. (c) Same cross section as above showing the calculated coseismic deformation near the Pitáycachi rupture segment. The displacements are exaggerated by a factor of 5000. From Suter & Contreras (2002).

Readjustments of tectonic stress during postseismic periods can last months to years (Pollitz and Cattania, 2017) because postseismic stresses, resulting from afterslip and viscoelastic relaxation of lower crust, change slowly. Thus, crustal stress is time dependent and must correlate with long-lasting seismicity after major earthquakes. Time-dependent seismicity models developed by Toda *et al.* (2005) in Southern California also indicate that background seismicity, due to static stress changes, can affect seismicity for decades.

SEISMICITY RECORDED DURING 2002-2011

The location of the earthquakes recorded by RESNES was first determined from the arrival times of *P* and *S* waves and a standard location procedure with the computer code Hypoinverse (Klein, 2002). There are important clusters of seismicity in areas with major mining operations like Cananea in the northern region; near Nacozari, in the central region; and near Mulatos in the southeast. Mine blasts that occurred within the schedule of mining activities were eliminated from the dataset. Nevertheless, some of the left-over events in these regions may have been caused by mining operations. The remaining events were relocated using the source-specific station term (SSST) method (Richards-Dinger and Shearer, 2000). Only the best relocated earthquakes, with rms <1 sec and with focal depths h > 2 km, were kept for further analysis to avoid possible random quarry blasts. All the final relocated events have hypocenters above 30 km and approximately half of them were located between 5 and 15 km depth (Castro, 2015).

The final relocated and filtered earthquakes originating near the fault system that ruptured in 1887 are displayed in Figure 10. Most events align along the traces of the main faults, Pitáycachi (P), Teras (T) and Otates (O). However, two major faults, located farther south, Villa Hidalgo (V) and Granados (G), also show seismic activity in the

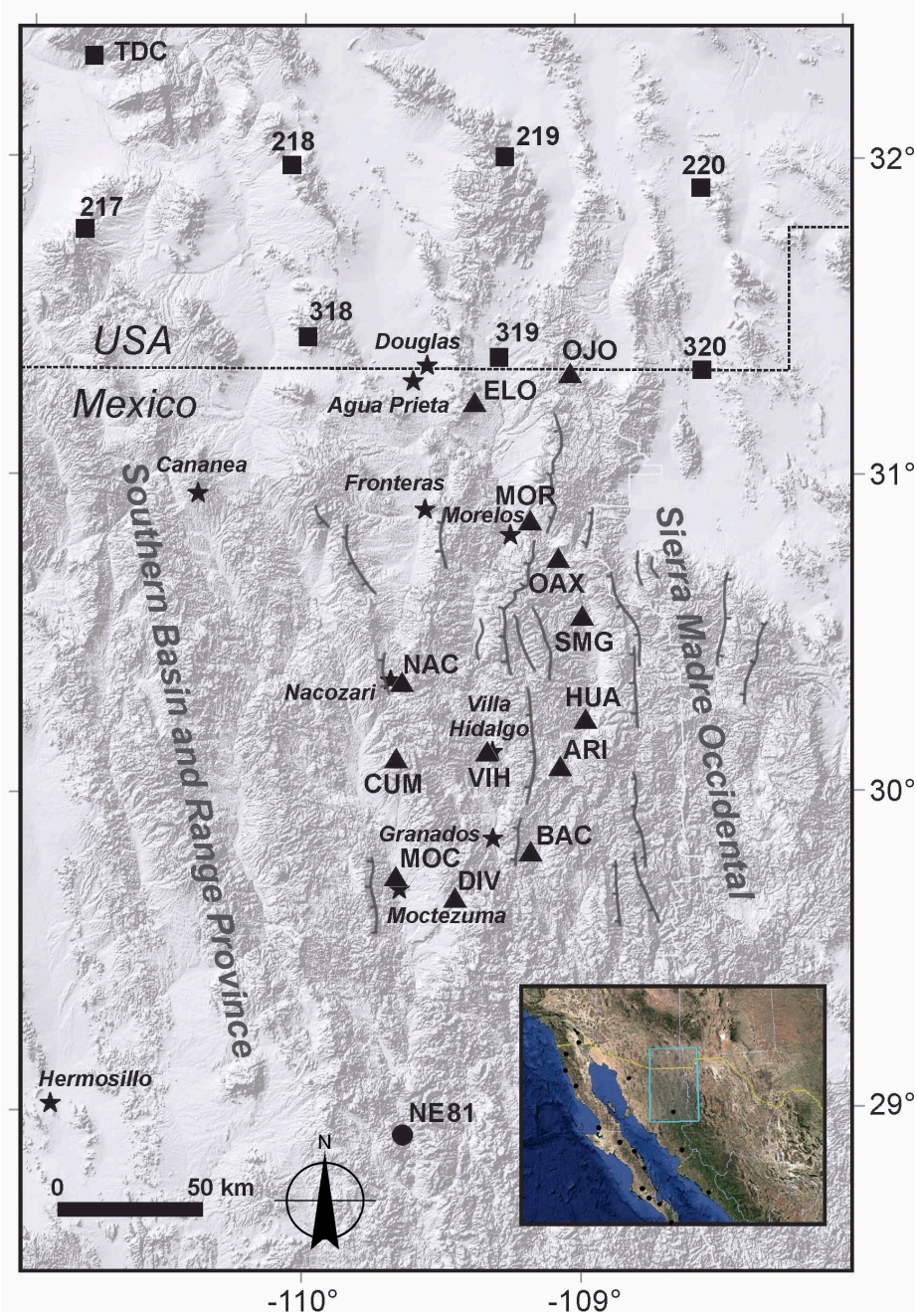

Figure 8. Location map showing the stations of the RESNES array (triangles) and USArray stations (squares). NE81 (circle) is a broadband station of the RESBAN-NARS network. Also shown are the traces of Basin and Range Province faults.

region where two devastating earthquakes occurred in 1913 and 1923 (see above). This can be due to an increase in failure stress induced by the 1887 rupture, as suggested by Suter and Contreras (2002). Alternatively, the 1887 rupture may have extended farther south than its mapped surface trace.

ESTIMATION OF LOCAL MAGNITUDE

The relocated earthquakes near the faults that ruptured in 1887 were used by Villalobos-Escobar and Castro (2015) to determine empirical relations to estimate their local magnitude (M_L). The hypocentral distances of these events vary between 9 and 190 km, their local magnitudes are in the range of 0.5 – 3.5, and their focal depths are less than 40 km.

Because the duration of the seismograms is approximately independent of epicentral distance and azimuth (Aki and Chouet, 1975), Villalobos-Escobar and Castro (2015) found the following relation between local magnitude and earthquake duration:

$$M_L = 3.14 \log \tau - 2.9526 \quad (1),$$

where M_L is the local magnitude and τ the duration measured in seconds from the first *P*-wave arrival until the signal-to-noise ratio of the *S*-wave coda equals three.

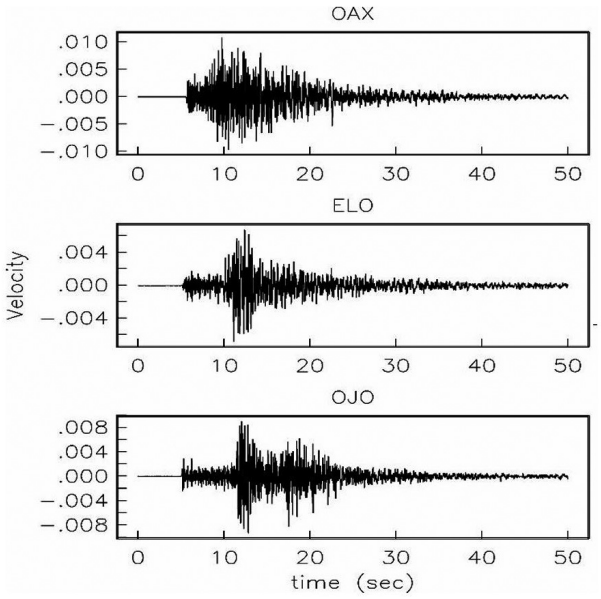

Figure 9. Representative seismograms recorded by stations OAX, ELO, and OJO (Figure 8) of an earthquake that originated on the Pitáycachi fault.

SEISMIC ATTENUATION IN NORTHEASTERN SONORA

Data from the RESNES array permitted, for the first time, to specify the attenuation of seismic waves in northeastern Sonora. Castro *et al.* (2008) obtained with this data set regional attenuation functions that describe how the spectral amplitudes of *P* and *S* waves decay with hypocentral distance. They found that the decay of the spectral amplitudes is faster near the rupture zone of the 1887 earthquake than in the surrounding area.

The attenuation curves obtained by Castro *et al.* (2008) were modeled in terms of physical parameters such as the quality factor *Q*, the geometrical spreading *G(r)*, and the high-frequency near-site attenuation parameter κ_0. *Q* is a useful physical parameter to characterize the attenuation because it measures the intrinsic and the scattering attenuations in the propagation media. This parameter is sensitive to changes of the elastic rock properties due to tectonic stress and the presence of fluids. These authors found that near the 1887 rupture zone, the *Q*-value of *P*-waves ($Q_P = 20.8\, f^{1.1}$) is smaller than that of *S* waves ($Q_S = 83.8 f^{0.9}$), indicating that *P* waves attenuate more than *S* waves in the frequency range from 0.6 to 63.1 Hz.

Castro *et al.* (2009) also studied the attenuation of body waves near the rupture area of the 1887 earthquake with a two-layer model. They found that in the lower crust the internal friction and the scattering are less severe than in the upper crust; consequently, seismic waves traveling in the upper crust attenuate more. They also observed that at high frequencies ($f > 8$ Hz), *Q* in the lower crust shows a weak frequency dependence, which suggests that the higher temperature there and the ductility of the deeper rocks reduce the body-wave scattering and the total attenuation.

Villalobos-Escobar and Castro (2014) derived a *Q* function for *S* waves for northeastern Sonora ($Q_S(f) = 141\, f^{0.74}$), which closely matches the *Q* function reported by Jeon and Herrmann (2004) for the Basin and Range Province in Utah, USA ($Q_S(f) = 160\, f^{0.75}$). This similarity suggests a close connection between the tectonic setting and the attenuation properties observed both in the northern and southern regions of the Basin and Range Province, highlighting the role of crustal structure in controlling seismic wave attenuation.

An alternative approach to characterizing the attenuation by a two-layer model is by ray-tracing the *S*-wave with a known velocity model. Castro and Villalobos-Escobar (2021) used this technique and found that within the first kilometer of the model $Q(f) = 127\, f^{0.7}$ and in the second layer, with a depth between 1 and 21 km, $Q(f) = 181\, f^{0.7}$ in the frequency range of 0.5–20 Hz.

THE SPECTRAL DECAY PARAMETER KAPPA

Kappa (κ), as defined by Anderson and Hough (1984), is another useful attenuation parameter that measures the high-frequency rate of decay of acceleration spectral amplitudes. Fernández *et al.* (2010) calculated κ using earthquakes located near the Pitáycachi fault and the RESNES stations. They found that κ increases with distances up to 80 km and decreases in the range of 80–100 km, which indicates that the attenuation of *S*-waves is higher at shallow depths. This observation is consistent with the attenuation results obtained by Castro *et al.* (2009) with a two-layer model, which shows less attenuation in the lower crust. Fernández *et al.* (2010) also determined the attenuation near the recording sites (κ_0) of the RESNES stations and found an average value of $\kappa = 0.04$ sec, and that κ_0 depends on the erosion degree of the near-surface rocks and other factors like fracturing rather than the rock type.

The measured values of κ are the sum of three attenuation components that can be represented as (Anderson, 1991; Ktenidou *et al.*, 2014; Castro *et al.*, 2022):

$$\kappa(\kappa_S, r, \kappa_0) = \kappa_S + \tilde{\kappa}(r) + \kappa_0 \qquad (2),$$

where κ_S is the near-source attenuation, $\tilde{\kappa}(r)$ is the regional average attenuation along the *S*-wave source- station distance *r*, and κ_0 is the near-site attenuation. Castro and Villalobos-Escobar (2020) estimated κ_S from earthquakes located in the epicentral area of the 1887 Sonora earthquake (Figure 11) and found that earthquake sources north of the Otates fault exhibit higher attenuation ($\kappa_S = 0.03$ sec) compared to those in the south, which have a value of $\kappa_S = 0.01$ sec, or three times smaller. One possible explanation is that the rock damage during the 1887 rupture was greater north of the Otates fault, making the quality factor *Q* lower compared to the southern region. An alternative explanation is that *Q* is higher in the south because the tectonic stress is higher in that region because it was not released during the 1887 event or because the rupture induced additional stress in the south due to directivity effects.

SEISMIC ENERGY RADIATED BY EARTHQUAKES NEAR THE RUPTURE OF THE 1887 MAIN SHOCK

The seismic energy radiated by the microseismicity located in the rupture area of the 1887 earthquake permitted to identify zones in the epicentral region of this major earthquake where tectonic stress appears to be accumulating. Castro and Villalobos-Escobar (2020) used a spectral inversion technique to retrieve the velocity source spectra of 47 earthquakes located in that region to estimate the seismic energy radiated by those events. They estimated that the average apparent stress of those earthquakes is low (0.0521 MPa), which is expected for the Basin and Range Province, where extensional tectonics dominate. They also found that the events that radiated the highest seismic energy are located in the stepover between the Otates and Teras segments of the 1887 rupture (Figure 12). They observed that in that zone there is a change in the strike direction of the faults (Figure 1) that may contribute to the accumulation of tectonic stress.

RECENT SEISMICITY

After the operation of RESNES, which recorded until 2011, there was a major recurrence of seismic activity in the region of the 1887 surface rupture between 2016 and 2021, with 11 events of magnitude ≥2.5 (Table 3, Figure 13; source: comprehensive earthquake catalog, ComCat of the U.S. Geological Survey). The sequence initiated with three events 2016-2018 in the north-central part of the Pitáycachi 1887 rupture segment (events 1 to 3 in Figure 13) with magnitudes between 3.0 and 3.7 (Table 3), followed by a magnitude 3.4 earthquake in 2018 farther south, in the center part of the Teras 1887 rupture segment (event 4 in Figure 13). The activity then migrated in 2019 to the northern tip of the Pitáycachi segment (events 5 and 6 in Figure 13 with magnitudes 3.7 and 3.5 respectively) and from there in 2020 to a region somewhat north of the Pitáycachi segment, inside Arizona (three events with magnitudes between 2.8 and 3.5). It then moved from there approximately 130 km south, to the southern part of the Otates segment, where a M_w 5.2 shock originated 31 July 2021 (Figures 1 and 13, event 7). This earthquake likely was the strongest one in the epicentral region of the 1887 main shock since the 1923 M_I 5.7 Granados-Huásabas earthquakes (see above). The slip vector orientation inferred from its focal mechanism is comparable to the orientation of the slickenlines measured on the Otates segment of the 1887 surface rupture (Figure 1, Table 2). A very similar focal mechanism (strike: 173°; dip: 51°; rake -76°) is provided in a report about this earthquake by the Servicio Sismológico Nacional (2021), which places the epicenter somewhat farther south, near the southern part of the Villa Hidalgo fault. Besides numerous aftershocks (including events 8 to 11 in Figure 13), four M 3.1–3.5 events occurred during the following two weeks approximately 100 km farther north, in the Animas Mountains of New Mexico (Ben-Horin and Pearthree, 2021, figs. 2 and 3). The timing suggests that these events were triggered by the 2021 main shock in the Otates fault region.

It is noteworthy that this recent seismic burst not only is limited to the general area of the 1887 rupture but also is distributed all along its strike. It likely partly occurred on minor faults within the crustal zone that was deformed in 1887 and partly was triggered on neighboring faults. These are obviously aftershocks of the 1887 main shock. Their

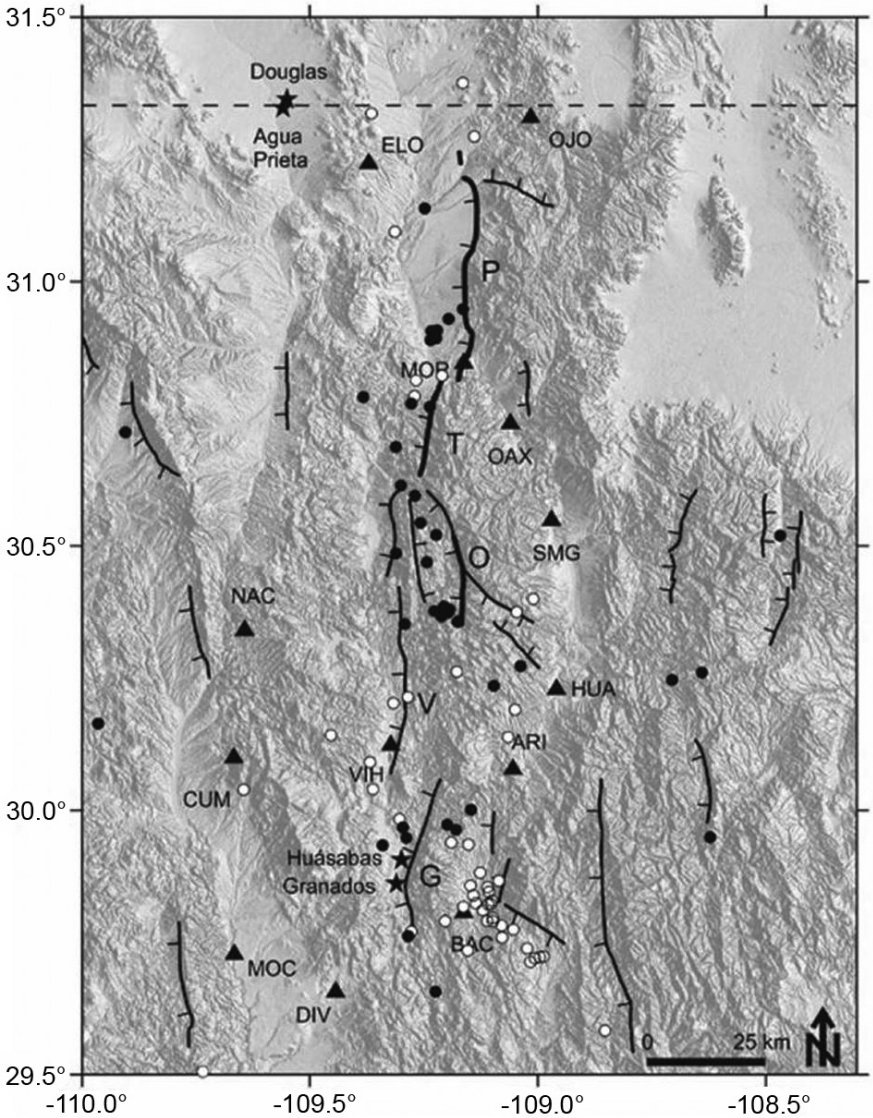

Figure 10. Relocated earthquakes that occurred in the period 2003-2007 (black circles) and 2008-2011 (white circles) near the fault system that ruptured in 1887 (modified from Castro, 2015). The marked fault traces are Pitáycachi (P), Teras (T), Otates (O), Villa Hidalgo (V), and Granados (G).

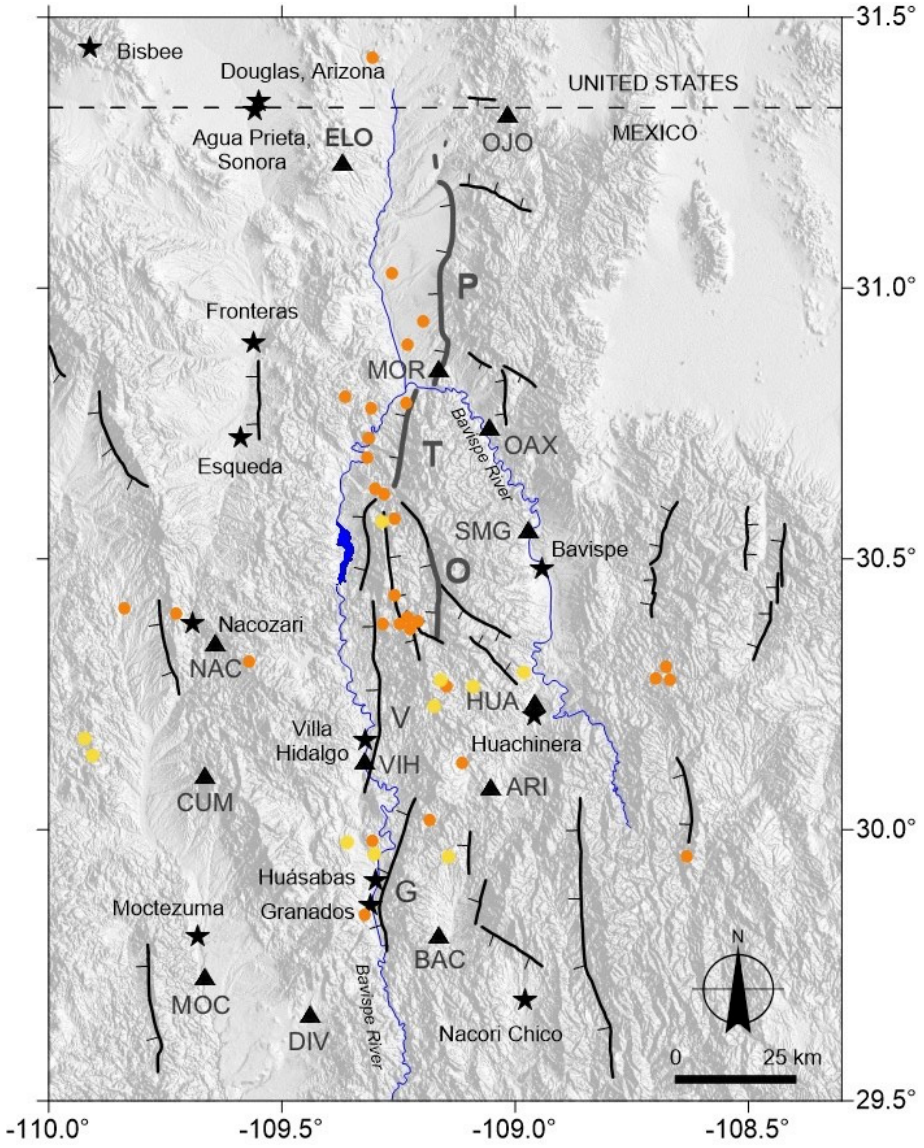

Figure 11. Epicentral locations and estimates of near-source attenuation (κ_S). Yellow dots are earthquakes with κ_S=0.01sec and orange dots are earthquake sources with κ_S=0.03 sec. Modified from Castro and Villalobos-Escobar (2020).

long duration can be explained by the unusually large magnitude of the 1887 main shock and by the low slip rates and long mainshock recurrence times of the faults that ruptured in 1887 (Table 2) (Castro *et al.*, 2010, and references therein).

CONCLUSIONS

We provide a map of the surface rupture of the 3 May 1887 Sonora earthquake (Figure 1) and define the rupture displacement profile. According to our detailed field work, the rupture extends significantly farther to the south than previously mapped by others, which led to a reassessment of the magnitude of this event, now estimated as M_w 7.5. This makes the 1887 earthquake the largest historical earthquake of the southern Basin and Range tectonic-physiographic province. Furthermore, this earthquake produced worldwide the longest recorded normal-fault surface rupture in historic time. The 1887 rupture extends over three first-order range-bounding Basin and Range Province normal faults (from south to north: Otates, Teras, and Pitáycachi), and has a maximum vertical displacement of 5.2 m and a length of 102 km. It is characterized at the surface and at focal depth by extensional dip slip on 55° to 72°W dipping faults and additionally by a minor left-lateral strike-slip component on the Teras and Pitáycachi segments. Disregarding the two minor Víbora rupture segments, the rupture was arrested in the north as well as in the south at major cross faults, and the surface offset profile tapers rapidly toward these faults. A 2.5-km-wide, unbreached right step-over separates the Pitáycachi and Teras segments of the surface rupture. This step-over is also defined by a minimum in the 1887 slip distribution, which suggests that Pitáycachi and Teras are independent rupture segments that do not merge at depth. The segment boundary between the Teras and Otates faults is characterized by a basement ridge, which, at its surface, was not breached by the 1887 rupture. The rupture kinematics and epicenter of the 1887 earthquake can be inferred from the bidirectional branching pattern observed along the trace of the Pitáycachi segment. The rupture likely originated on

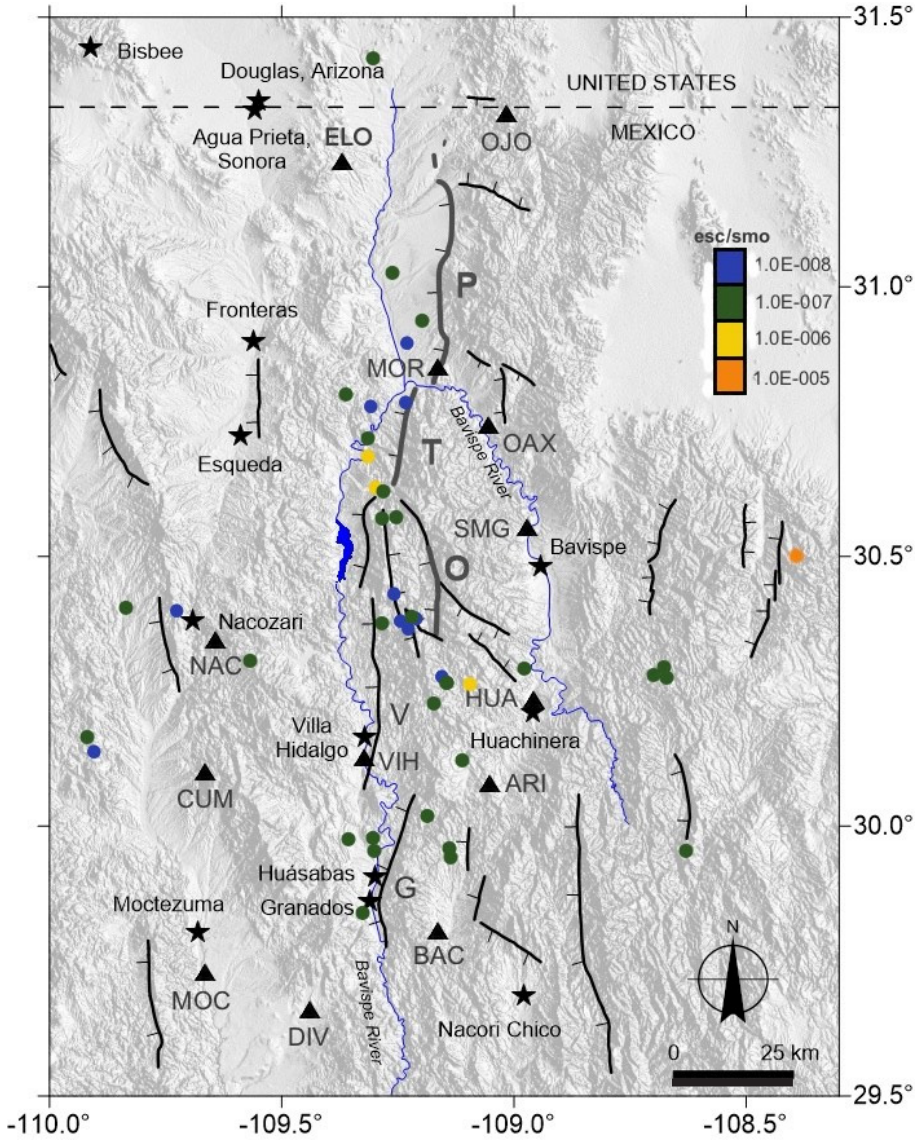

Figure 12. Epicentral locations of events (circles) used to estimate the seismic energy. The different colors indicate the value of the radiated energy scaled with the seismic moment (esc/smo). Modified from Castro and Villalobos-Escobar (2020).

Table 3. Earthquakes in northeastern Sonora between 2012 and 2025 with magnitudes ≥2.5.

Reference	Origin time (UTC)	Location	Epicenter		Depth (km)	Magnitude (M)
			Long. (°W)	Lat. (°N)		
1	2016-12-01; 02:26:19	28 km ENE of Fronteras	109.281	30.981	11.5	3.7
2	2017-08-26; 23:47:40	33 km SE of Agua Prieta	109.263	31.161	18.0	3.0
3	2018-01-31; 04:30:06	35 km ENE of Fronteras	109.236	31.047	14.2	3.0
4	2018-02-27; 06:53:47	32 km E of Esqueda	109.249	30.724	10.0	3.4
5	2019-10-11; 01:10:54	49 km E of Douglas	109.031	31.297	10.0	3.7
6	2019-10-11; 01:36:32	48 km ESE of Douglas	109.049	31.253	10.0	3.5
7	2021-07-31; 21:19:12	17 km W of Bavispe	109.120	30.453	10.0	5.2
8	2021-08-01; 22:40:09	30 km WNW of Bavispe	109.239	30.576	14.0	2.5
9	2021-08-10; 18:34:21	19 km WNW of Huachinera	109.145	30.281	15.7	3.1
10	2021-08-18; 12:33:54	23 km NNE of Villa Hidalgo	109.190	30.345	10.1	4.1
11	2021-09-26; 00:17:45	14 km NNE of Villa Hidalgo	109.239	30.270	10.0	4.1

The earthquakes epicenters are plotted and referenced in Figure 13.Source: U.S. Geological Survey, Comprehensive Earthquake Catalog (ComCat). A focal mechanism of event 7 is plotted on Figure 1, and its parameters are included in Table 2.

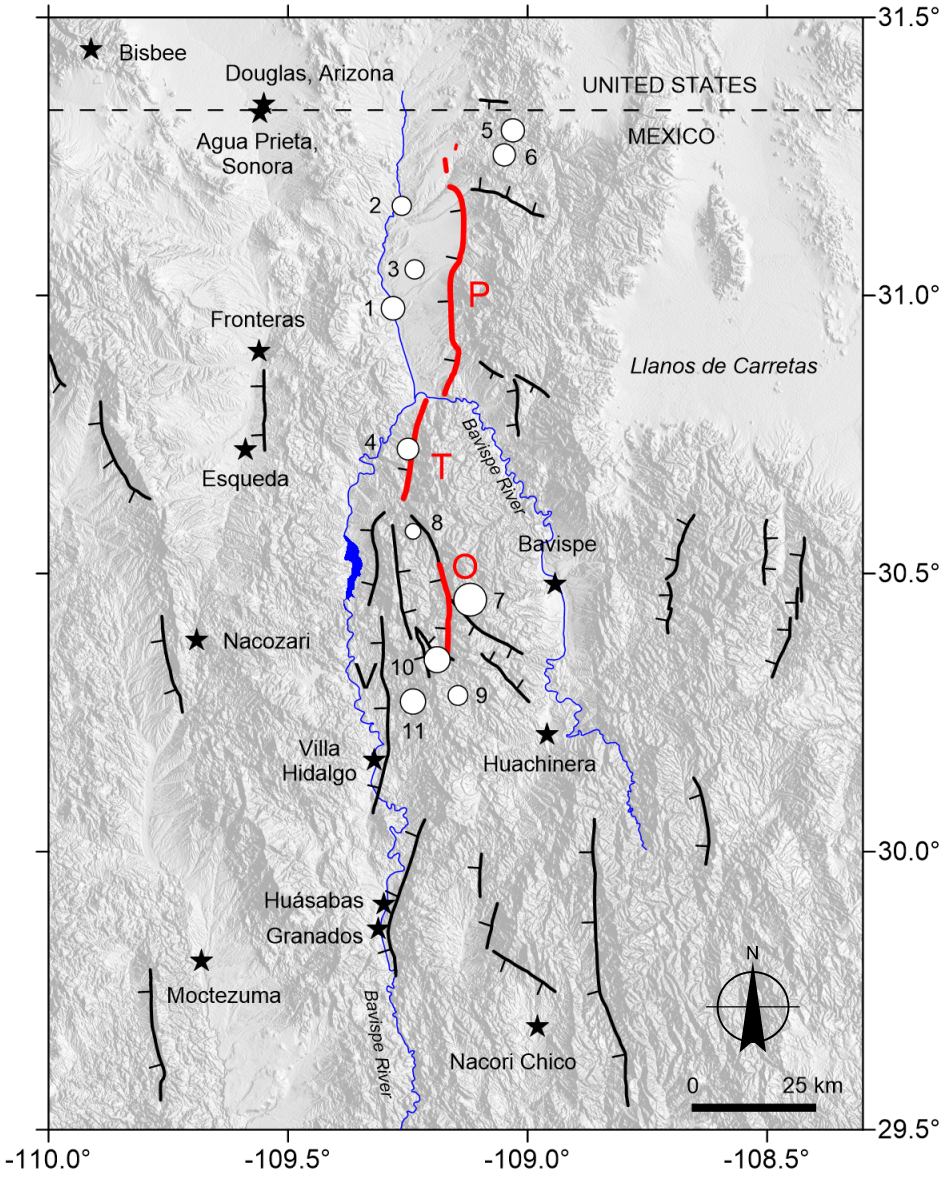

Figure 13. Earthquakes with magnitudes ≥2.5 (white circles) that originated in the epicentral region of the 1887 surface rupture between 2016 and 2021 (Source: U.S. Geological Survey, Comprehensive Earthquake Catalog, ComCat). Their reference numbers (Table 3) are in chronological order. The radii of the circles are proportional to the magnitudes of the events. Pitáycachi (P), Teras (T), and Otates (O) are segments of the 1887 surface rupture (marked in red). V: Villa Hidalgo fault.

the Pitáycachi fault, propagated bilaterally along this fault, and then jumped to the Teras, and from there to the Otates fault. Coulomb stress modeling suggests that stress increases caused by singularities at the tips of the three rupture segments triggered seismicity in the step-over between the northern and central segments of the 1887 surface rupture, as well as in the Granados-Huásabas region, to the south of the documented surface rupture.

The observational geological data served as a base for the lay-out of a regional seismic network in the epicentral region of the 1887 earthquake, named *Red Sísmica del Noreste de Sonora* (RESNES). The array, which was installed in 2002 and operated until 2011, consisted of nine digital autonomous seismological stations. Its recordings indicate ongoing microseismicity not only along the faults that ruptured in 1887, but also along two major Basin and Range Province normal faults located farther south, in the Granados-Huásabas region. In addition to the parametric data of the seismicity distribution, the high quality of the RESNES digital recordings permitted the characterization of the regional seismic attenuation and a spatial analysis of the seismic energy radiated by the recorded earthquakes.

Acknowledgments. We thank Arturo Pérez Vertti and Antonio Mendoza for station maintenance, data acquisition, data preprocessing, and distribution of RESBAN data. Their participation in the RESNES project is appreciated. We also thank the anonymous reviewers for their comments and suggestions which helped us to improve the manuscript.

Author contributions. All the authors were directly involved in the formation of this manuscript. Raúl R. Castro, Gina P. Villalobos-Escobar, and Oscar Romero are responsible for the installation and operation of the seismic network, and the collection, analysis and interpretation of the recorded data; Juan Contreras for the Coulomb modeling; and Max Suter for the manuscript parts related

to earthquake geology, historical seismology, and seismotectonics.

Data and resources. Besides the data included in this paper, much additional information can be found in the numerous referenced publications that resulted from this project. RESNES recordings are available per request from the first author. Our maps and measurements are included in the database of 75 historical surface-rupturing earthquakes from global shallow crustal settings, created within the Fault Displacement Hazard Initiative (FDHI), which is publicly available for download from the Dataverse platform at the University of California, Los Angeles (UCLA) through the following URL: https://doi.org/10.25346/S6/Y4F9LJ (Sarmiento *et al.*, 2025; Bozorgnia et al., 2025). Our 1887 surface rupture data are also included in the SURE 2.0 worldwide surface rupture database of historical earthquakes (Nurminen *et al.*, 2022). Facsimiles of documents about the 1913 and 1923 earthquakes that devastated Granados and Huásabas, preserved at Archivo General del Estado de Sonora, are available at https://www.researchgate.net/publication/265381297_1913_Huasabas_Earthquake and https://www.researchgate.net/publication/265383838_1923_Granados_-_Huasabas_Earthquake, respectively. A facsimile of the 1886 macroseismic questionnaire used by the U.S. Geological Survey for the 1887 Sonora earthquake (Suter, 2025) is available at https://osf.io/6xm48/. The parameters of the 2021 focal mechanism graphed in Figure 1 were culled from the Global Centroid Moment Tensor (Global CMT) catalog at https://www.globalcmt.org/. The data in Table 3 were culled from the Comprehensive Earthquake Catalog (ComCat) of the U.S. Geological Survey at https://earthquake.usgs.gov/data/comcat/. The stereoplots in Figure 1 were graphed with the program FAULTKINWIN by Richard Allmendinger (https://www.rickallmendinger.net/faultkin), which was also used to calculate the parameters of their P- and T-axes using the linked Bingham method. All websites were last accessed in October 2025.

Declaration of competing interests. The authors declare that they have no known competing financial interests or personal relationships that could have influenced the work reported in this article.

Funding. This project was made possible in part by financial and logistic support from *Universidad Nacional Autónoma de México* (UNAM) and the former *Consejo Nacional de Ciencia y Tecnología* (CONACYT, Grant Number G33102-T).

REFERENCES

Aguilera, J. G. (1888). Estudio de los fenómenos séismicos del 3 de mayo de 1887. *Anales del Ministerio de Fomento de la República Mexicana*, *10*, 5–56. https://www.biodiversitylibrary.org/item/183548#page/11/mode/1up

Aki, K., & Chouet, B. (1975). Origin of coda waves: source, attenuation, and scattering effects. *Journal of Geophysical Research*, *80*(23), 3322–3342. https://doi.org/10.1029/JB080i023p03322

Aki, K., & Richards, P. G. (2002). *Quantitative Seismology: Theory and Methods* (2nd ed.). University Science Books.

Anderson, J. G. (1991). A preliminary descriptive model for the distance dependence of the spectral decay parameter in southern California. *Bulletin of the Seismological Society of America, 81*, 2186–2193.

Anderson, J. G., & Hough, S. E. (1984). A model for the shape of the Fourier amplitude spectrum of acceleration at high frequencies. *Bulletin of the Seismological Society of America, 74,* 1969–1984.

Bahat, D. (1982). Extensional aspects of earthquake induced ruptures determined by an analysis of fracture bifurcation. *Tectonophysics, 83*, 163–183. https://doi.org/10.1016/0040-1951(82)90017-8

Ben-Horin, J. Y., & Pearthree, P. A. (2021). Recent seismic excitement in the area of the 1887 Great Sonoran Earthquake. *Arizona Geology e-Magazine*. https://blog.azgs.arizona.edu/blog/2021-09/recent-seismic-excitement-area-1887-great-sonoran-earthquake

Berglund, H. T., Sheehan, A. F., Murray, M. H., Roy, M., Lowry, A. R., Nerem, S., & Blume, F. (2012). Distributed deformation across the Rio Grande Rift, Great Plains, and Colorado Plateau. *Geology, 40*, 23–26. https://doi.org/10.1130/G32418.1

Bouchbinder, E., Fineberg, J., & Marder, M. (2010). Dynamics of simple cracks. *Annual Review of Condensed Matter Physics, 1,* 371–395. https://doi.org/10.1146/annurev-conmatphys-070909-104019

Bozorgnia, Y., Abrahamson, N., Baize, S., Boncio, P., Chen, R., Chiou, B., Dawson, T., Kottke, A., Kuehn, N., Lavrentiadis, G., Madugo, C., Madugo, D., Milliner, C., Moss, R., Nurminen, F., Sarmiento, A., Thomas, K., Thompson, S., Valentini, A., Visini, F., & Zandieh, A. (2025). Fault Displacement Hazard Initiative research program. *Earthquake Spectra*, *41*(4), 2679–2690. https://doi.org/10.1177/87552930251356418

Broek, D. (1986). *Elementary Engineering Fracture Mechanics* (4th revised ed.). Martinus Nijhoff Publishers.

Broerman, J., Bennett, R. A., Kreemer, C., Blewitt, G., & Pearthree, P. A. (2021). Geodetic extension across the southern Basin and Range and Colorado Plateau. *Journal of Geophysical Research: Solid Earth, 126*, e2020JB021355. https://doi.org/10.1029/2020JB021355.

Bull, W. B., & Pearthree, P. A. (1988). Frequency and size of Quaternary surface ruptures of the Pitáycachi fault, northeastern Sonora Mexico. *Bulletin of the Seismological Society of America, 78*, 956–978.

Castro, R. R. (2015). Seismicity in the Basin and Range Province of Sonora, México, between 2003 and 2011, near the rupture of the 3 May 1887 Mw 7.5 earthquake. *Geofísica Internacional*, *54*, 83–94. https://doi.org/10.1016/j.gi.2015.04.004

Castro, R.R., & Villalobos-Escobar, G. (2020). Seismic energy radiated by earthquakes in the Basin and Range Province of Sonora, Mexico, near the rupture of the 1887 M_w7.5 earthquake. *Journal of Seismology*, *25*(1), 73-83. https://doi.org/10.1007/s10950-020-09953-0

Castro, R. R., & Villalobos-Escobar, G. (2021). Upper Crust Attenuation in the Basin and Range Province of Sonora, Mexico. *Journal of Seismology*, *25*, 1241–1249. https://doi.org/10.1007/s10950-021-10025-0.

Castro, R. R., Romero, O. M., & Suter, M. (2002). Red Sísmica para el monitoreo de la sismicidad del sistema de fallas normales del noreste de Sonora, *GEOS*, *22*, 379.

Castro, R. R., Condori, S. C. Romero, O. Jacques, C, & M. Suter, M. (2008). Seismic attenuation in northeastern Sonora, Mexico. *Bulletin of the Seismological Society of America, 98*, 722–732.

Castro, R. R., Huerta, C. I., Romero, O., Jacques, C., Hurtado, A., & Fernández, A. I. (2009). Body-wave attenuation near the rupture of the 1887 Sonora, Mexico, earthquake (Mw 7.5). *Geofísica Internacional*, *48*, 297–304. https://doi.org/10.22201/igeof.00167169p.2009.48.3.27

Castro, R., Shearer, P. M., Astiz, L., Suter, M., Jacques-Ayala, C., & Vernon, F. (2010). The long-lasting aftershock series of the 3 May 1887 M_w 7.5 Sonora earthquake in the Mexican Basin and Range Province. *Bulletin of the Seismological Society of America, 100*, 1153–1164.

Castro, R. R., Colavitti, L., Vidales-Basurto, C. A., Pacor, F., Sgobba, S., & Lanzano, G. (2022). Near-source attenuation and spatial variability of the spectral decay parameter kappa in Central Italy. *Seismological Research Letters*, *93*(4), 2299–2310. https://doi.org/10.1785/0220210276

Clayton, R. W., Trampert, J., Rebollar, C. J., Ritsema, J., Persaud, P., Paulssen, H., Pérez-Campos, X., van Wettum, A., Pérez-Vertti, A., & diLuccio, F. (2004). The NARS-Baja array in the Gulf of California rift zone. *Margins Newsletter*, *13*, 1–4.

Dieterich, J. H. (1994). A constitutive law for rate of earthquake production and its application to earthquake clustering. *Journal of Geophysical Research, 99*, 2601–2618.

DuBois, S. M., & Smith, A. W. (1980). *The 1887 Earthquake in San Bernardino valley, Sonora, Historic accounts and intensity patterns in Arizona* (Special Paper 3). Arizona Bureau of Geology and Mineral Technology. https://repository.arizona.edu/handle/10150/630009

DuRoss, C. B., Personius, S. F., Crone, A. J., Olig, S. S., Hylland, M. D., Lund, W. R., & Schwartz, D. P. (2016). Fault segmentation: New concepts from the Wasatch Fault Zone, Utah, USA. *Journal of Geophysical Research Solid Earth, 121,* 1131–1157. https://doi.org/10.1002/2015JB012519

Fernández, A. I., Castro, R. R., & Huerta, C.I. (2010). The spectral decay parameter Kappa in northeastern Sonora, Mexico. *Bulletin of the Seismological Society of America, 100*, 196–206.

Figueroa, J. (1970). *Catálogo de sismos ocurridos en la República Mexicana*. Universidad Nacional Autónoma de México. Instituto de Ingeniería, UNAM, Reporte 272, 88 pp.

González-León, C. M., Valencia, V. A., López-Martínez, M., Bellon, H., Valencia-Moreno, M., & Calmus, T. (2010). Arizpe sub-basin: A sedimentary and volcanic record of Basin and Range extension in north-central Sonora, Mexico. *Revista Mexicana de Ciencias Geológicas, 27*(2), 292–312.

Gutenberg, B., & Richter, C. F. (1949). *Seismicity of the Earth and associated phenomena*. Princeton University Press, Princeton, New Jersey, 273 pp.

Hatem, A. E., Reitman, N. G., Briggs, R. W., Gold, R. D., Thompson Jobe, J. A., & Burgette, R. J. (2022). Western U.S. Geologic Deformation Model for Use in the U.S. National Seismic Hazard Model 2023. *Seismological Research Letters, 93*(6), 3053–3067. https://doi.org/10.1785/0220220154

Jeon, Y. S., & Herrmann, R. B. (2004). High-frequency earthquake ground-motion scaling in Utah and Yellowstone. *Bulletin of the Seismological Society of America*, *94*, 1644–1657.

King, G. C. P., Stein, R. S., & Lin J. (1994). Static stress changes and the triggering of earthquakes. *Bulletin of the Seismological Society of America, 84*, 935–953.

Klein, F. W. (2002). *User's guide to HYPOINVERSE-2000, a Fortran program to solve for earthquake locations and magnitudes* (Open-File Report, 02–171). U.S. Geological Survey.

Ktenidou, O-J., Cotton, F., Abrahamson, N. A., & Anderson, J. G. (2014). Taxonomy of *κ:* a review of definitions and estimation approaches targeted to applications. *Seismological Research Letters*, *85*, 135–146.

Liang, S., Zhang, G., Xu, Z., Liu, J., Li, H., Shi, J., & Zhou, Y. (2022). Aftershocks triggering in a conjugate normal fault zone: A case study of the 2020 Mw 5.7 Utah earthquake sequence. *Natural Hazards*, *114*(1), 1059–1078. https://doi.org/10.1007/s11069-022-05382-z

Lockridge, J., Fouch, M., & Arrowsmith, J R. (2012). Seismicity within Arizona during the deployment of the EarthScope USArray Transportable Array. *Bulletin of the Seismological Society of America*, *102*(4), 1850–1863. https://doi.org/10.1785/0120110297

Natali, S. G., & Sbar, M. L. (1982). Seismicity in the epicentral region of the 1887 northeastern Sonora earthquake, Mexico. *Bulletin of the Seismological Society of America, 72*, 181–196.

Nurminen, F., Baize, S., Boncio, P., Blumetti, A. M., Cinti, F. R., Civico, R., & Guerrieri, L. (2022). SURE 2.0 – New release of the worldwide database of surface ruptures for fault displacement hazard analyses. *Scientific Data*, *9*, article 729. https://doi.org/10.1038/s41597-022-01835-z

Pearthree, P. A., Bull, W. B., & Wallace, T. C. (1990). Geomorphology and Quaternary geology of the Pitáycachi fault, northeastern Sonora, Mexico. In G. E. Gehrels, & J. E. Spencer (Eds.), *Geologic excursions through the Sonoran Desert region, Arizona and* Sonora (Special Paper 3, pp. 124–135). Arizona Geological Survey.

Pollitz, F. F., & Cattania, C. (2017). Connecting crustal seismicity and earthquake-driven stress evolution in Southern California. *Journal of Geophysical Research*, *Solid Earth*, *122*, 6473–6490. https://doi.org/10.1002/2017JB014200

Richards-Dinger, K., & Shearer, P. (2000). Earthquake locations in southern California obtained using source-specific station terms. *Journal of Geophysical Research*, *105*, 10939–10960. https://doi.org/10.1029/2000JB900014

Romero, O. M., Jaques, C., & Castro, R. R. (2004). Análisis de la Sismicidad detectada por la red sismológica del noreste de Sonora. *GEOS, 24*, 230.

Sarmiento, A., Madugo, D., Shen, A., Dawson, T., Madugo, C., Thompson, S., Bozorgnia, Y., Baize, S., Boncio, P., Kottke, A., Lavrentiadis, G., Mazzoni, S., Milliner, C., Nurminen, F., & Visini, F. (2025). Database for the Fault Displacement Hazard Initiative. *Earthquake Spectra*, *41*(4), 2721–2745. https://doi.org/10.1177/87552930241262766

Sbar, M. L., & DuBois, S. M. (1984). Attenuation of intensity for the 1887 northern Sonora, Mexico earthquake. *Bulletin of the Seismological Society of America, 74*, 2613–2628.

Schwartz, D. P. (2018). Past and future fault rupture lengths in seismic source characterization – the long and short of it. *Bulletin of the Seismological Society of America, 108*(5A), 2493–2520. https://doi.org/10.1785/0120160110.

Sharon, E., & Fineberg, J. (1999). Confirming the continuum theory of dynamic brittle fracture for fast cracks. *Nature, 397*, 333–335. https://doi.org/10.1038/16891

Sharon, E., Gross, S. P., & Fineberg, J. (1995). Local crack branching as a mechanism for instability in dynamic fracture. *Physical Review Letters, 74*, 5096–5099. https://doi.org/10.1103/PhysRevLett.74.5096

Servicio Sismológico Nacional. (2021). *Reporte especial: Secuencia sísmica del 13 de marzo al 26 de agosto de 2021, Sonora (M 5.1)*. Servicio Sismológico Nacional. http://www.ssn.unam.mx/sismicidad/reportes-especiales/2021/SSNMX_rep_esp_20210811_secuenciaSonora_M51.pdf

Sumner, J. R. (1977). The Sonora earthquake of 1887. *Bulletin of the Seismological Society of America*, *67*, 1219–1223.

Suter, M. (2001). The historical seismicity of northeastern Sonora and northwestern Chihuahua, Mexico (28-32° N, 106-111° W). *Journal of South American Earth Sciences*, *14*, 521-532. https://doi.org/10.1016/S0895-9811(01)00050-5

Suter, M. (2006). Contemporary studies of the 3 May 1887 M_W 7.5 Sonora, Mexico (Basin and Range Province) earthquake. *Seismological Research Letters, 77*, 134–147. https://doi.org/10.1785/gssrl.77.2.134

Suter, M. (2008a). Structural configuration of the Otates fault (southern Basin-and-Range Province) and its rupture in the 3 May 1887 M_W 7.5 Sonora, Mexico earthquake. *Bulletin of the Seismological Society of America, 98*, 2879–2893. https://doi.org/10.1785/0120080129

Suter, M. (2008b). Structural configuration of the Teras fault (southern Basin-and-Range Province) and its rupture in the 3 May 1887 M_W 7.5 Sonora, Mexico earthquake. *Revista Mexicana de Ciencias Geológicas, 25*(1), 179–195.

Suter, M. (2015). Rupture of the Pitáycachi Fault in the 1887 M_W 7.5 Sonora, Mexico earthquake (southern Basin-and-Range Province): Rupture kinematics and epicenter inferred from rupture branching patterns. *Journal of Geophysical. Research: Solid Earth, 120*, 617–641. https://doi.org/10.1002/2014JB011244

Suter, M. (2020). Comment on "Active crustal deformation in the Trans-Mexican volcanic belt as evidenced by historical earthquakes during the last 450 years" by G. Suárez et al. *Tectonics, 39*, e2019TC006016. https://doi.org/10.1029/2019TC006016

Suter, M. (2025). Early macroseismic intensity observations, isoseismal maps, and instrumental recordings of earthquakes in Mexico (1888–1934): A Review. *Seismological Research Letters, 97*(1), 564–577. https://doi.org/10.1785/0220250157

Suter, M., & Contreras, J. (2002). Active tectonics of northeastern Sonora, Mexico (southern Basin and Range Province) and the 3 May 1887 M_W = 7.4 earthquake. *Bulletin of the Seismological Society of America, 92*, 581–589. https://doi.org/10.1785/0120000220

Suter, M., & Morelos-Rodríguez, L. (2024). Seismotectonics of the Querétaro region (central Mexico) and the 1934 M_I 4.8 earthquake north of Celaya. *Seismological Research Letters, 95*(2A), 820–833. https://doi.org/10.1785/0220230256

Suter, M., & Morelos-Rodríguez, L. (2025). Seismotectonics of north-central Mexico (Basin and Range Province) and the 3 April 1925 M_I 4.9 Chalchihuites, Zacatecas, earthquake. *Seismological Research Letters, 96*(4), 2152–2166. https://doi.org/10.1785/0220240475

Suter, M., Carrillo-Martínez, M., & Quintero-Legorreta, O. (1996). Macroseismic study of shallow earthquakes in the central and eastern parts of the trans-Mexican volcanic belt, Mexico. *Bulletin of the Seismological Society of America, 92*, 1952–1963.

Taggart, J., & Baldwin, F. (1982). Earthquake sequence of 1938-1939 in Mogollon Mountains, New Mexico. *New Mexico Geology, 4*, 49–52.

Trampert, J., Paulsen, H., van Wettum, A., Ritsema, J., Clayton, R., Castro, R., Rebollar, C., & Pérez-Vertti, A. (2003). New array monitors seismic activity near the Gulf of California in México. *EOS, Transactions of the American Geophysical Union, 84,* 29–32.

Toda, S., Stein, R. S., Richards-Dinger, K., & Bozkurt, S. B. (2005). Forecasting the evolution of seismicity in Southern California: Animations built on earthquake stress transfer. *Journal of Geophysical Research*, *110*(B5). https://doi.org/10.1029/2004JB003415

U.S. Geological Survey (2025). *Quaternary fault and fold database for the United States*. U.S. Geological Survey. https://www.usgs.gov/natural-hazards/earthquake-hazards/faults

Villalobos-Escobar, G. P., & Castro, R. R. (2014). S-wave attenuation in northeastern Sonora, Mexico, near the faults that ruptured during the earthquake of 3 May 1887 Mw7.5. *SpringerPlus, 3*(1), 747. https://doi.org/10.1186/2193-1801-3-747

Villalobos-Escobar, G. P., & Castro, R. R. (2015). Estimation of local magnitude in northeastern Sonora, Mexico, using empirical relations based on recorded duration. *Seismological Research Letters, 86*, 870–875. https://doi.org/10.1785/0220140027

Wallace, T. C., & Pearthree, P. A. (1989). Recent earthquakes in northern Sonora. *Arizona Geology, 19*(3), 6–7.

Wells, D. L., & Coppersmith, K. J. (1994). New empirical relationships among magnitude, rupture length, rupture width, rupture area, and surface displacement. *Bulletin of the Seismological Society of America, 84*, 974–1002.

Young, J., & Pearthree, P. (2014). Duncan M 5.3 earthquake of June 2014 and temporary seismic network deployment, *Arizona Geology e-Magazine,* https://azgeology.azgs.arizona.edu/article/seismic/2014/10/duncan-m53-earthquake-june-2014-and-temporary-seismic-network-deployment